Development of real-time, quantitative free fatty acid uptake assays for adipose tissue explants using fluorescence and microfluidics

by

Tesfagebriel Mihretab Hagos

A thesis submitted to the Graduate Faculty of
Auburn University
In partial fulfillment of the
Requirements for the Degree of
Master of Science in Analytical Chemistry

Auburn, Alabama
May 7, 2017

Key Words: free fatty acid, microfluidics, uptake, 3D-printing, fluorescence, microplate

Approved by

Christopher J. Easley, Chair, Knowles Associate Professor of Chemistry
Curtis G. Shannon, Hunt Professor of Chemistry and Chairman
Wei Zhan, Associate Professor of Chemistry

Abstract

Free fatty acid (FFA) uptake by adipocytes in response to nutritional or hormonal stimuli is a key process in the complex metabolic cascade leading to diabetes and obesity. The work presented in this thesis is focused on developing analytical tools to quantify free fatty acid uptake by mouse adipocytes in real time. Two approaches were used to quantify the uptake kinetics of free fatty acids.

Chapter 1 talks about general concepts of fatty acid uptake and previous approaches with their benefits and drawbacks. Chapter 2 introduces and examines the first approach in our project, which is quantifying free fatty acid uptake dynamics in primary adipocytes using customized micro-wells made with 3D-printed templates. In chapter 3 a more sensitive, simple, inexpensive fluorescence based microfluidic assay was developed to achieve a real-time quantitative BODIPY-FFA uptake measurement. We employed a fluorescently labeled FFA analog, BODIPY-hexadecanoic acid (i.e. BODIPY-palmitic acid or BODIPY-FFA), to directly follow FFA uptake by adipocyte tissue explants under various treatments using a multi-channel microfluidic device. A five channel microfluidic chip was used, with two central channels to interrogate adipocyte tissue explant. At the same time, three calibration channels were analyzed as a novel method of real-time calibration. Explants were treated with BODIPY-FFA as the fluorescence intensity was measured downstream using a fluorescence microscope for quantification. Unlike traditional techniques like quencher based technique (QBT), flow cytometry, or radioactive fatty acids which rely on end-point readout, our system allows us to

flow the reagents continuously over the adipocyte tissue therefore mimicking the physiological environment. With this system, we were able to quantify free fatty acid uptake by adipocytes in real-time with minimal optical drift and without exposing cells to direct excitation light. We have also used the system to simultaneously measure BODIPY-FFAC12 and the glucose analogue 2-NBDG (2-(N-(7-Nitrobenz-2-oxa-1, 3-diazol-4-yl) Amino)-2-Deoxyglucose) uptake kinetics in adipose tissue explants. Finally, chapter 4 outlines future plans to fully automate the system using valving in order to allow rapid, real-time quantification of FFA uptake dynamics in adipose tissue explants.

Acknowledgments

I would like to thank all the people who contributed in some way to the work described in this thesis. First, I thank my academic advisor, Professor Christopher J. Easley, for accepting me into his group. He contributed to an enjoyable graduate school experience by giving me intellectual freedom in my work, engaging me in new ideas, every time pushing my limits and demanding a high quality of work in all my endeavors. I have learned many things, not only in Academia but life in general. I believe the experience of graduate school has shaped me in ways I would never have achieved otherwise. I also want to thank my committee members, Professor Curtis G. Shannon, and Professor Wei Zhan who offered guidance and support.

I would like to thank the Auburn University Department of Chemistry and Biochemistry for giving me the opportunity to do my master's work. It would have not been possible had it not been for their gracious award of assistantship. The results in this thesis were accomplished with the help and support of fellow lab mates and friends. I would like to thank everyone in the Easley group: Dr. Joonyul Kim, Dr. Adriana Avila, Dr. Jessica Brooks, Subramaniam Somasundaram, Jean Negou, Xianpeng Li, Mark Holtan, Katarena Ford, Juan Hu, and Niamat Khuda.

I want to thank my wife Semhar Mussie, who has been by my side every minute since we met. Her love and confidence in me gave me courage to dream bigger and keep moving. I am also greatly indebted to my family members, to my precious sister Nebiat Mihretab Hagos, the greatest person I know, and to whom I owe everything I achieved in life. I was inspired by her hard work, resilience and energy, her truly moving spirit, but most of all her unwavering and

unconditional love and support through the years. I want to recognize my siblings, Senait, Tirhas, Maria, Yonas, Luchia, Furtuna, my wonderful nieces, Selam and Ariam and numerous friends who endured this long process with me, always offering support and love.

Table of Contents

List of Tables

List of Figures

List of Abbreviations

BAT	Brown Adipose Tissue
BODIPY	Boron-Dipyrromethene
BODIPY-FFA	BODIPY-labeled palmitic acid or BODIPY-labeled lauric acid
CD36	Cluster of Differentiation-36
FFA	Free Fatty Acid
LCFA	Long Chain Fatty Acid
PDMS	Polydimethylsiloxane
QBT	Quencher Based Technology
TAG	Triacylglycerol or Triglyceride
WAT	White Adipose Tissue
WHO	World Health Organization

CHAPTER ONE

Introduction

1.1 Research Motivation

In 2004, Liao et al. published an article on real-time quantification of non-esterified long chain fatty acid uptake in to cells using a clever idea, leveraging a fluorescently labelled fatty acid (BODIPY-FFA) and cell-impermeable quencher[1]. He uses a detector positioned beneath the plate which measures intracellular fluorescence. This method was safe and simple, however cells needed to be plated (seeded) in a microplate and were directly exposed to an excitation source which could have effects on fluorescence readout and cell viability. Through the years many publications have emphasized the qualitative aspect of fatty acid uptake. The quantitative uptake assays available include indirect detection of conversion of fatty acids across the plasma membrane or direct tracing of labeled fatty acids. Indirect methods include measurement of intracellular TAG stores. A disadvantage to this method is TAG stores are also driven by many other processes including lipolysis, fatty acid catabolism, LCFA efflux, and de novo synthesis[2].

An alternative strategy by Kampf et al used Acrylodan labeled Intestinal Fatty Acid Binding Protein (ADIFAB) probe, which in the absence of unbound free fatty acids, fluoresces in the blue at 432 nm. Unfortunately fluorescent binding proteins are unable to distinguish exogenous from endogenous LCFAs. Furthermore this approach requires microinjection of cells which prevents in-vivo measurements[3,4].

Direct assays use ^{14}C and ^{3}H radiolabeled fatty acids or fatty acid analogs conjugated to fluorescent or bioluminescent probes. They have the advantage of faithfully mimicking the biochemical properties of natural fatty acids. Their disadvantages include use of radioactive materials, the lack of dynamic monitoring of cellular uptake, and high costs that limit their use in

High throughput applications. Fluorescently labeled fatty acid analogs, particularly C1-BODIPY C12, and BODIPY FL C16 have proven to be suitable alternatives to radiolabeled long-chain fatty acids (LCFAs). Another appealing aspect of these BODIPY labeled FFAs is their ability to participate in downstream metabolic reactions following uptake[2,5].

Our approach has been two-fold. In the first project our aim was to develop a simple, fluorescence-based method for quantitative FFA uptake without the disadvantage of phototoxicity. We use customized micro-wells made with 3D-printed templates to quantify free fatty acid uptake by 3T3-L1 adipocytes. In the second project we exploit advantages of microfluidic technology to develop a real-time, quantitative free fatty acid uptake assay in adipose tissue-explants.

1.2 Obesity and Adipose tissue

Increased adipose tissue mass is the primary phenotypic characteristic of obesity. Obesity, defined by the WHO as abnormal or excessive fat accumulation that may impair health, increases risks for multiple metabolic diseases, such as type 2 diabetes, cardiovascular disease and several types of cancer. According to the WHO fact sheet, obesity has more than doubled worldwide since 1980. In 2014, more than 1.9 billion adults, 18 years and older, were overweight. Of these over 600 million were obese. 39% of adults aged 18 years and over were overweight in 2014, and 13% were obese. Most of the world's population lives in countries where excess weight and obesity kills more people than underweight. 42 million children under the age of 5 were overweight or obese in 2013[6].

Primarily, obesity and excess weight are caused by a dysregulation of the fat storage process, which causes a larger proportion of consumed calories to be stored in the fat tissue. Adipose tissue, which is composed mostly of adipocytes by volume, is a major endocrine organ and plays

a key role in energy homeostasis. Conventionally two types of adipose tissue, white adipose tissue (WAT) and brown adipose tissue (BAT) have been known to exist in humans and other animals. Recent literature discovered the presence of brown adipose tissues (BAT) in adult humans.

White adipocytes are derived from mesenchyma or pericyte whereas brown adipocytes originate from myogenic lineage or trans-differentiation from white adipocytes (brown-in-white or "brite" adipocytes). Although its link with adaptive thermogenesis, body weight or metabolic disorders in humans has not been proven yet, BAT plays critical role in cold-induced thermogenesis. Lee et al reports, while the quantity of gluteofemoral adipose tissue is protective, increases in upper body adipose tissue (visceral and abdominal subcutaneous) present an independent risk. In practice, obesity does not depend on body weight but depends on either the number of white adipocytes or the amount of WAT. WAT functions primarily to store excess energy in the form of triglycerides (TGs). In contrast, BAT oxidizes fuels and dissipates energy in the form of heat, hence WAT and BAT have opposing roles in obesity. This begs the question whether, understanding of the regulation and mechanisms of adipose tissues including FFA uptake and storage can potentially open the way to treating obesity-associated metabolic diseases.

Anatomically, WAT is distributed throughout the body including many isolated storehouses. Fat stores are highly variable, ranging from 5 to 60% of total body weight. Subcutaneous adipose tissues (SAT) store >80% of total body fat in the body. BAT is primarily distributed around interscapular, axillary, paravertebral, and perirenal sites. Typically brown fat is located in interscapular (upper back region) and perirenal (around the kidney) sites in rodents and large mammals including humans[7,8,9].

1.3 Fatty acids

According to IUPAC Compendium of Chemical Terminology (Gold Book) fatty acids are aliphatic monocarboxylic acids derived from or contained in esterified form in an animal or vegetable fat, oil or wax[10].

Until recently they were considered as metabolic intermediates with no biological effects. They are now known to exert biological effects by activation of particular G protein–coupled receptors (GPCRs). FFAs can be classified according to their chain length as short-chain fatty acids (SCFAs), which have 1–6 carbon atoms; medium-chain fatty acids (MCFAs), which have 7–12 carbon atoms; and long-chain fatty acids (LCFAs), which have more than 12 carbon atoms[11].

1.3.1 Fatty acid biosynthesis from Acetyl CoA

In the formation of different chain-length fatty acids, Acetyl CoA undergoes a carboxylation reaction to produce malonyl CoA in the presence of citrate. This step is the rate limiting step which determines fatty acid synthesis. Before entering the synthase complex cycle, an acyl carrier protein (ACP) which acts as flexible arm that carries growing fatty acid chain from active site to active site is introduced. This is a common physiological theme, namely the need for protein-based carriers of fatty acid chains due to their limited solubility in aqueous solution.

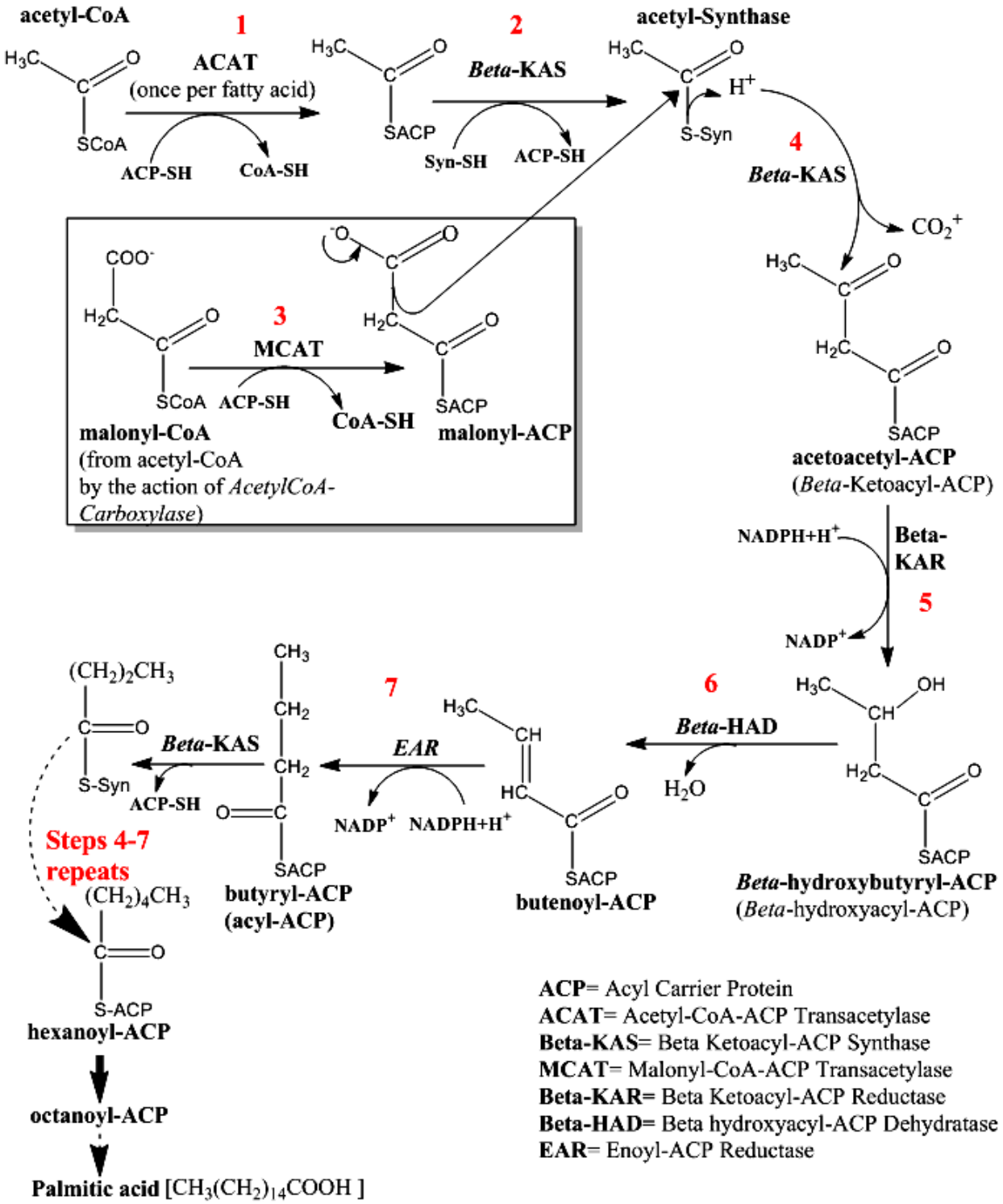

Fig.1.1 Fatty acid biosynthesis
Modified from [12]

Once butyryl-ACP is produced as in Fig.1:1, it reenters the cyclic synthesis chain, becoming equivalent to acetyl-CoA and the process is repeated for multiple rounds until C16 palmitoyl-ACP is formed. Palmitic acid is then cleaved as a final step of this chain of reactions[12].

1.3.2 Relationship of free fatty acid with obesity and insulin resistance

It is now well known that, not only does adipose tissue stores and releases fatty acids but also synthesizes and releases a large number of other active compounds[13,14].This understanding has provided a conceptual framework which helps to understand how obesity can result in the development of insulin resistance. Accordingly, an expanding fat mass releases increasing amounts of compounds such as FFA, angiotensin 2, resistin, TNF-α, interleukin 6, interleukin 1-β and others. Some of these compounds, when infused in large amounts, can produce insulin resistance. Some crucial observations with FFAs have established the physiological link between obesity and insulin resistance. It has been reported that plasma FFA levels are elevated in most obese individuals[15], raising plasma FFA levels increases insulin resistance[16] and lowering of FFA improves insulin resistance[17].

1.4 Fatty acid analogues and their bioanalytical applications

Boron-dipyrromethene (BODIPY) is an intensely fluorescent fluorophore. The BODIPY core Fluorophore is 4, 4-difluoro-4-bora-3a, 4a-diaza-s-indacene. This zwitterionic fluorophore was first synthesized by Treibs and Kreuzer in 1968[18]. BODIPY fluorophore probes have various applications in cell biology and biophysics. This fluorophore family is intrinsically lipophilic, therefore are more likely to imitate the properties of natural lipids. BODIPY lipid probes have excellent spectral properties which include long wavelength range (Excitation maxima; 500 nm to ~650 nm, Emission maxima; 510 nm to ~665 nm), narrow spectral band width, small fluorescence stokes shift, high quantum yield (typically 0.9 in fluid phase lipid bilayers),

insensitivity to environment (fluorescence quantum yields of fatty acids are not diminished in water) high photostability, and high molar absorptivities (ε-max typically >80,000 $cm^{-1}M^{-1}$). The BODIPY group also carries no net charge which makes it a more reliable depth-dependent membrane probe than dansyl or nitrobenzoxadiazole (NBD)[19].

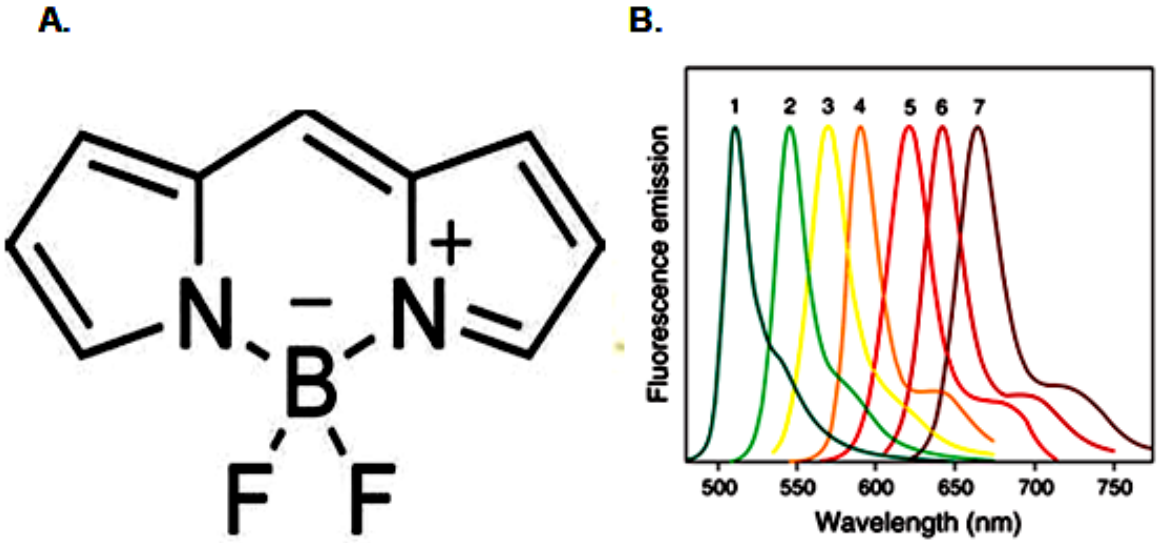

Fig.1.2 A) BODIPY core Fluorophore B) Normalized fluorescence emission spectra of (1) BODIPY FL, (2) BODIPY R6G, (3) BODIPY TMR, (4) BODIPY 581/591, (5) BODIPY TR, (6) BODIPY 630/650 and (7) BODIPY 650/665 fluorophores in methanol. From[19,20]

Stahl A. et al[21] employed C1-BODIPY C12 to demonstrate an insulin induced translocation of fatty acid transport protein which had enhanced effect on fatty acid uptake in 3T3-L1 Adipocytes. Hong Li et al[22] utilized C1-Bodipy C12 to screen fatty acid uptake inhibitors, where C1-BODIPY C12 was incubated with cells expressing FATP2 in a 96-well plate. The mmFATP2-dependent C1-BODIPY C12 uptake was monitored by measuring intracellular C1-BODIPY-C12 fluorescence on a microtiter plate reader, whereas extracellular fluorescence was quenched by a cell viability dye, trypan blue.

Varlamov et al[23] used BODIPY C12 to label adipocyte tissue explants to look at the differences in FFA uptake with respect to adipocyte cell size. They showed that adipose tissue within the

same animal and same anatomical location can comprise a heterogeneous population of adipocytes that differ in size and insulin sensitivity. Small adipocytes are found to be more insulin sensitive, whereas large adipocytes are typically less responsive. Somwar et al[24] used BODIPY FL C16 (labeled palmitate, or BODIPY-FFA) to track the exchange of intracellular lipids between adjacent lipid droplets (LDs) in differentiated 3T3-L1 adipocytes. They photo bleached selected lipid droplets (LDs) using targeted laser and observe fluorescence recovery in those LDs over time.

The use of fluorescent BODIPY-FFA C12allowed Chu et al[25], to identify novel cell biological features in unilocular adipocytes (most abundant cell type in WAT). Recently the Varlamov group discovered heterogeneity with respect to insulin-dependent uptake of FFAs and glucose by individual adipocytes residing within the same cell population. They have shown that FFA uptake in WAT and a mosaic pattern of fluorescence depended on the length of the aliphatic carbon chain attached to BODIPY, in that BODIPY C12 and BODIPY FL C16 entered the cLD in an insulin-dependent manner but displayed cellular heterogeneity in uptake, whereas BODIPY FL C16 was not efficiently transported into adipocytes[26].

1.4.1 Syntheses of BODIPY dyes

BODIPY dyes are considered as substitutes for fluorescein and rhodamine. 8-substituted BODIPY dyes can be synthesized through condensation of acyl chlorides with pyrroles, followed by complexation with $BF_3.Et_2O$ in the presence of a base (**Fig.1.3**)

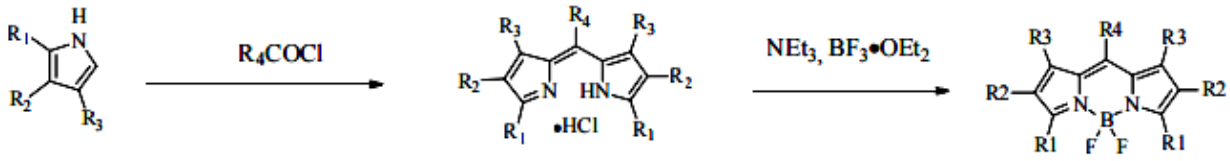

Fig.1.3 Synthesis of BODIPY dyes
Modified from[19]

1.5 Fatty acid uptake by adipocytes

Fatty acids are predominantly lipophilic; therefore it was originally presumed that they cross the lipid bilayer by diffusion. However, many organs and cell types exhibit a rapid, saturable, substrate-specific, and hormonally regulated LCFA uptake. The later indicate involvement of some form of protein mediated mechanism. For this reason the mechanism by which fatty acids especially long chain fatty acids (LCFA) cross plasma membrane has been a subject of debate for the last decade. Although predominantly protein mediated it is now known that both mechanisms are involved. Long-chain fatty acid (LCFA) is a crucial source of energy for cells. Uptake and activation of LCFA is important to many cellular processes, like membrane synthesis, intracellular signal transduction, energy metabolism, posttranslational modifications, and transcriptional regulation of metabolic genes[27,28].

In circulation, LCFA comes from two sources, either release from LCFA stores in adipose tissue or breakdown of triacylglycerol (TAG) rich lipoprotein particles by the action of lipoprotein lipase. Plasma LCFAs circulate bound to albumin, while in the intestine they form mixed micelles with bile acids.

LCFA uptake occurs in four main steps. First, localized generation of free fatty acids through various mechanisms and binding to albumin. Second fatty acid dissociation from albumin followed by binding to plasma membrane proteins, such as CD36, which continually hands the FFAs on to the fatty acid transport proteins (FATPs), Third transport across plasma membranes, and finally intracellular association with fatty acid binding and acyl-CoA binding proteins [29,30,31]. Subsequently they can participate in a variety of metabolic process such as mitochondrial β-oxidation and TAG synthesis[8,2,32].

Unbound FFAs also act extracellularly (**Fig.1.4A**) in stimulating the G-protein-coupled receptor GPR40 in β-cells to induce insulin secretion, or by activating toll-like receptors (TLRs) to initiate the innate immune response. Moreover, FFAs can act in the brain, in controlling the release of Agouti-related protein (AgRP) and neuropeptide Y (NPY) in the hypothalamus[33].

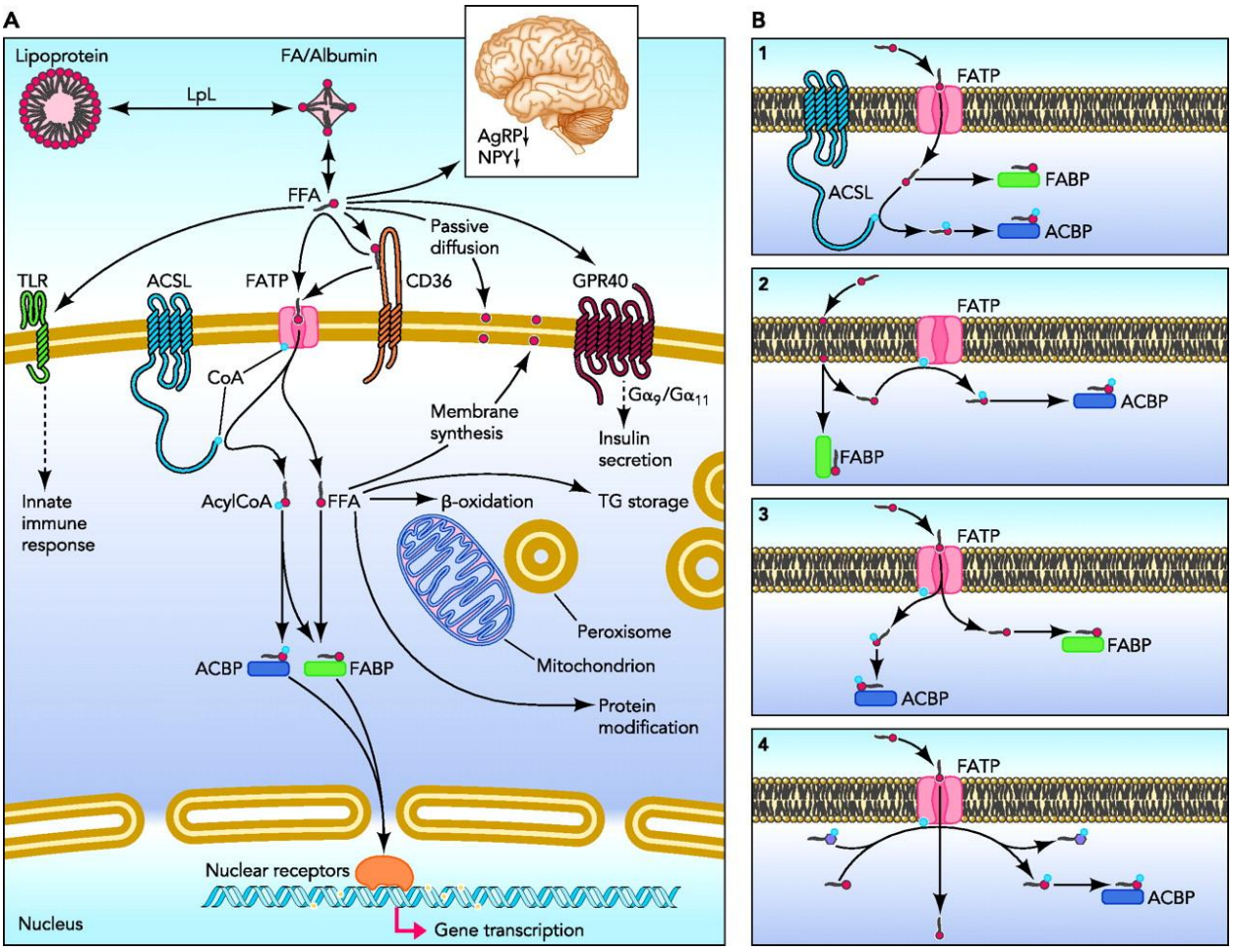

Fig.1.4 Free fatty acid uptake and action in mammalian cells: A) Generation of serum free fatty acids (FFA) from lipoproteins by the action of endothelial lipoprotein lipase (LpL) B) different hypotheses of protein-mediated FFA uptake[33].

There are four different theories (**Fig.1.4B**) describing the protein mediated uptake of FFAs, model-1 depicts FATPs as solely transmembrane transport proteins mediating fatty acid uptake, possibly in close association with other proteins like acyl-CoA synthetase long-chain family member 1 (ACSLs). Model-2 describes FATPs to be membrane-bound very-long-chain acyl-

CoA synthetases that trap fatty acid inside the cell following their diffusion across the plasma membrane. Model-3 shows, FATPs combine the transport with acyl-CoA synthetase activity and model-4 describes FATPs as being multifunctional proteins and mediate fatty acid uptake independently of their esterification activities[33].

Considerable research has been devoted to identifying proteins involved in the binding and transfer of LCFAs on the plasma membrane since the first report of such a protein by Barry et al in 1989. These researches lead to identification of the solute carrier family 27 (Fatty Acid Transport Proteins, FATPs), the scavenger receptor CD36, and the mitochondrial aspartate amino transferase (FABPpm). WAT expresses FATP1, FATP4, CD36, and FABPpm. Fatty acids take part in cellular energetics as well as insulin sensitivity and their uptake rates can be dynamically regulated. For this reason many techniques have been developed to determine LCFA uptake kinetics, especially by white adipose tissue (WAT)[34,35,36].

1.5.1 In vitro LCFA uptake

Approaches developed so far to determine LCFA uptake by adipocytes include indirect detection of transition of fatty acids across plasma membrane or direct tracing of labeled fatty acids. Measurement of cellular TAG stores is a prime example of indirect method. Nevertheless we cannot rely on this type of measurement because TAG stores are not only driven by cellular LCFA uptake but also by rates of lipolysis, fatty acid catabolism, LCFA efflux, and de novo synthesis from glucose and other substrates[2].

Another indirect method is the use of intracellular pH indicators. LCFA entry into vesicles was paralleled by a decrease in intravesicle pH, suggesting that the LCFA species that flip-flops across the membrane is the protonated fatty acid (FAH), which then dissociates to the fatty acid anion (FA-) and a proton. Fatty acid-induced proton fluxes across the plasma membrane are then

related to actual LCFA fluxes. However, a detailed study on brown adipose tissue by Fedorenko et al shows that unprotonated fatty acids can also be moved across membranes[37,38].

As an alternative strategy by Kampf uses acrylodan labeled Intestinal Fatty Acid Binding Protein (ADIFAB). In the absence of unbound free fatty acids, the ADIFAB probe fluoresces in the blue at 432 nm. In the presence of unbound free fatty acids, the emission shifts to green with a peak at 505 nm. The ratio of fluorescence at 505 nm and 432 nm allows concentration of unbound free fatty acids to be determined without further calibration. As shown in fig.1:5A, 3T3F442A adipocytes were microinjected with ADIFAB, the fluorescent probe of unbound FFA (FFAu). Phase contrast microscopy reveals the discrete lipid droplets characteristic of 3T3F442A cells (panel1). Fluorescence images were recorded at 435 and 505 nm. The ratio of the image intensities at 505 and 435 nm were used to determine intracellular FFA concentration [FFAi] and are represented using a false color scale (panels 2–8). The color scale bar in fig.1:5A indicates [FFAi] in nM. A disadvantage of this technique is that fluorescent binding proteins are unable to distinguish exogenous from endogenous LCFAs. In addition, this approach requires the microinjection of cells and is not convenient for in vivo measurements. This procedure however remains the only way to predict diseases such as ischemia[3,4].

Direct uptake assays take advantage of commercially available variety of ^{14}C and ^{3}H radiolabeled fatty acids or fatty acid analogs conjugated to fluorescent or bioluminescent probes. Although their biochemical properties are very similar to natural fatty acids, use of radioactive materials, lack of dynamic monitoring of cellular uptake, and high costs limit their use in high throughput applications. As previously mentioned fluorescently labeled fatty acid analogs, particularly C1-BODIPY C12, and BODIPY FL C16 were found to be appropriate alternatives to radiolabeled LCFAs[2,5].

Fluorescence-activated cell sorters (FACS) and plate readers are commonly used to quantify LCFA uptake. FACS can further be applied to measure cell size, surface markers, or cell viability in diverse cell populations. In contrast, plate reader based assays offer a higher throughput. Both methodologies depend on end-point readout. They also demand time consuming heterogeneous analysis involving washing steps. Instead combination of water soluble, cell impermeable, quenchers with fatty acid analogues, were used conveniently for real-time fatty acid uptake analysis[1].

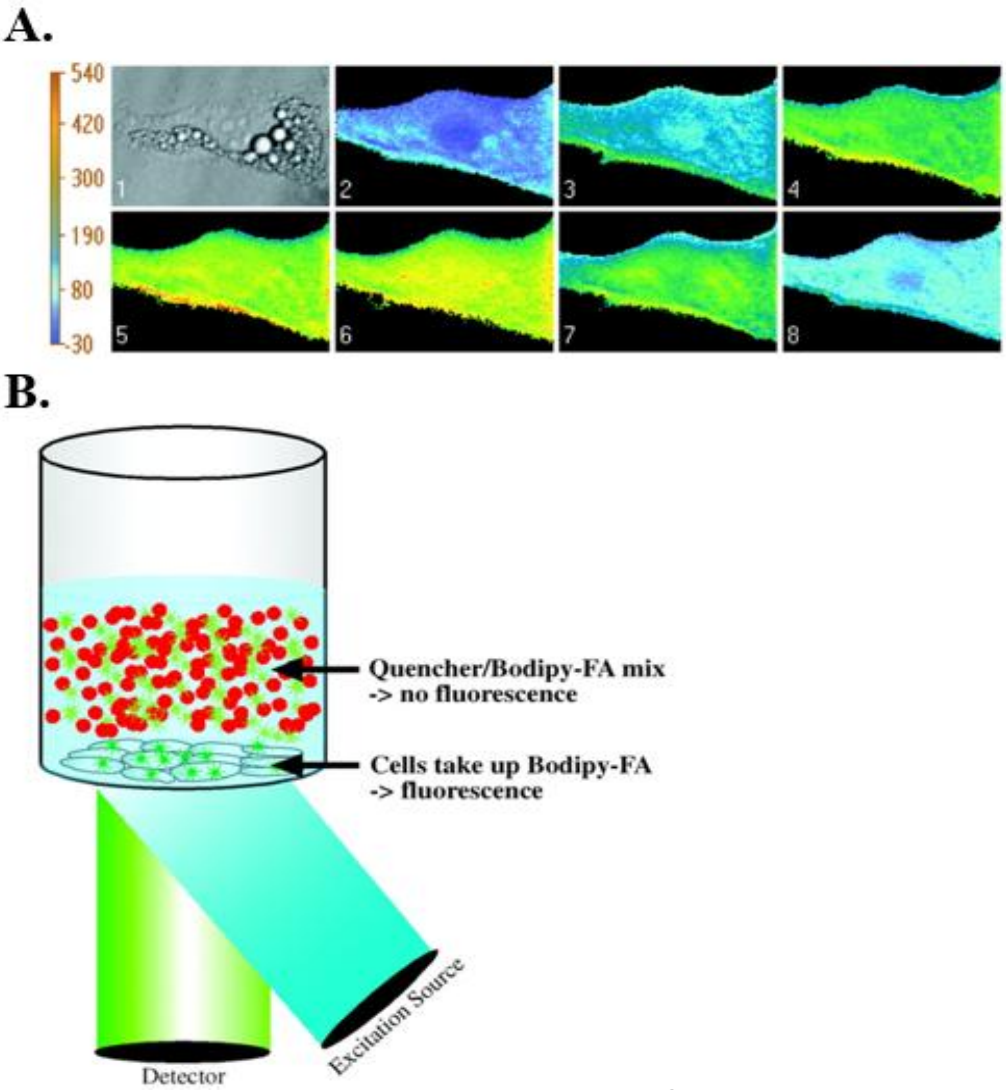

Fig.1.5 A) Intracellular FFA meassured by ADIFAB[3] B) Quencher based uptake; Instrumentation of one of the first attempts to quantify BODIPY-FFA uptake by adipocytes[1]

1‡ "This research was originally published in the Journal of lipid research. Liao, J.; Sportsman, R.; Harris, J.; Stahl, A. J. Lipid Res. 2005, 46 (3), 597–602. © The American Society for Biochemistry and Molecular Biology"

3‡ "This research was originally published in the Journal of biological chemistry. Kampf, J. P.; Kleinfeld, A. M. J. Biol. Chem. 2004, 279 (34), 35775–35780. © The American Society for Biochemistry and Molecular Biology"

In recent work by our group, a new technique of direct fatty acid uptake using microfluidics was developed. A customized microfluidic input/output multiplexer (μMUX) with 16 fluidic channels and 8 active microvalves for dynamic control over hormones and nutrients to/from endocrine tissues was fabricated. The device was automated through feedback sensing of solution level[39]. 3D-printed templates are used to interface both islets and adipose tissues[40].The device was proven functional by analyzing both islets and adipose tissue. For the adipose tissue fatty acid uptake analysis, an assay with similar mechanism to that shown in **Figure 1.5A** was developed, but in this case the carrier protein (BSA) was chemically labeled with a quencher molecule. In this way, only the fatty acids taken up by the cells would be sufficiently fluorescent for detection by microscopy.

1.5.2 In vivo LCFA uptake

In vivo LCFA uptake assays have been done in brown adipose tissue (BAT) in an effort to understand a link between its thermogenesis and body weight. LCFAs are however the predominant substrates for BAT uncoupled respiration[41].

A bioluminescent approach based on an activatable LCFA probe developed by Henkin et al offers a suitable approach to measure LCFA in vivo. The compound is taken up via physiological pathways by a transporter-mediated process, its disulfide bond reduced by intracellular glutathione, and resultant thiol undergoes cyclization releasing free luciferin. Luciferase-catalyzed conversion of luciferin to oxyluciferin produces a photon of light, which is detected using a charge-coupled device (CCD) camera. **Fig.1.6** show a schematic presentation of this process In the presence of luciferase, light generation is proportional to cellular fatty acid uptake[42,43].

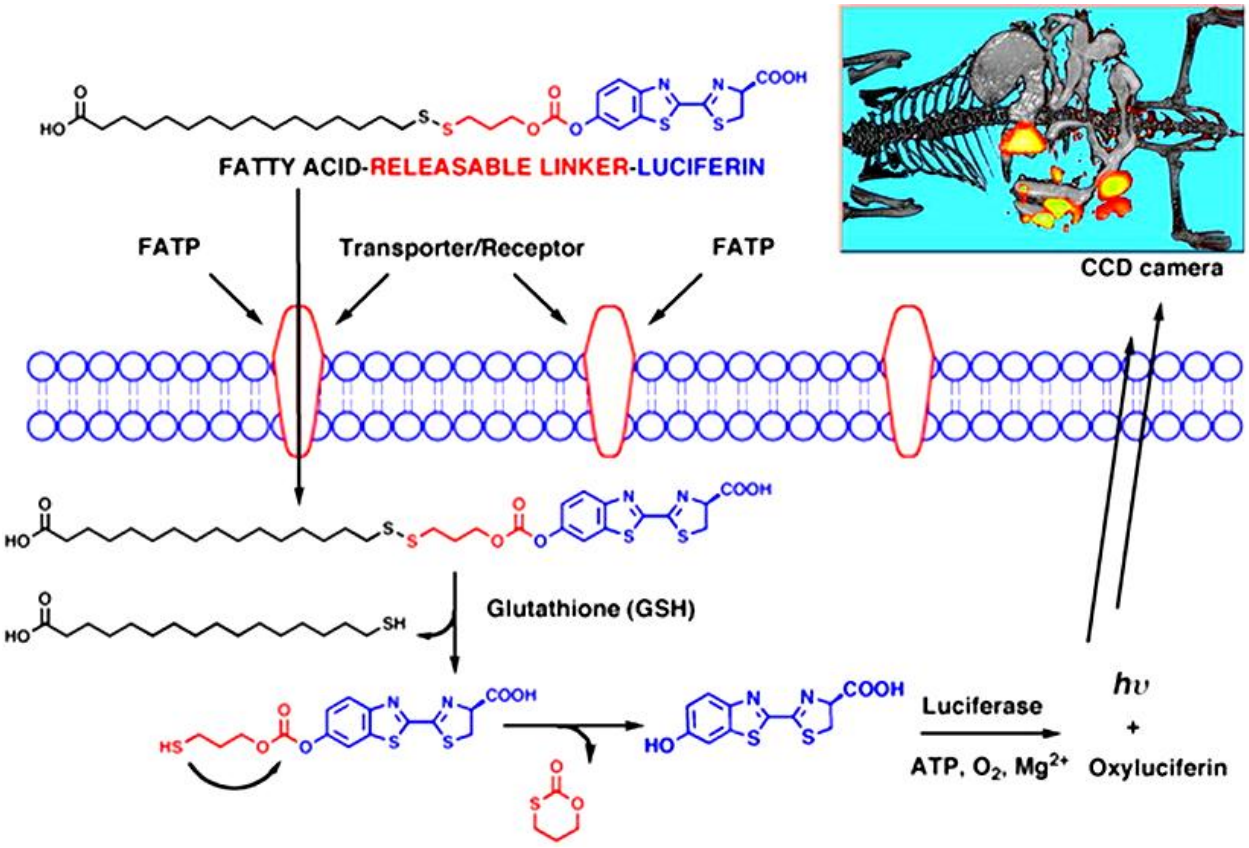

Fig.1.6 Strategy for bioluminescence imaging of fatty acid uptake

"Reprinted with permission from: Henkin, A. H.; Cohen, A. S.; Dubikovskaya, E. A.; Park, H. M.; Nikitin, G. F.; Auzias, M. G.; Kazantzis, M.; Bertozzi, C. R.; Stahl, A. *ACS Chem. Biol.* **2012**, *7* (11), 1884–1891. Copyright 2012 American Chemical Society"

CHAPTER 2

Quantifying free fatty acid uptake dynamics in 3T3_L1 adipocytes using customized micro-wells made with 3D-printed templates

2.1 Introduction

Photo toxicity and photo bleaching are the two most common problems encountered during imaging of live cells. Photo toxicity is a phenomenon whereby live cells undergo damaging physiological changes such as vacuolation, blebbing or even cell death during a direct exposure to exciting light. It is mainly the result of reactive oxygen species (ROS) from excited fluorophores. ROS can eventually undergo oxidation reaction with proteins, nucleic acids, lipids and fluorophores, leading to cell cycle arrest or cell death due to photo toxicity.

Jean-Yves reports that although often overlooked or ignored in fluorescence-based imaging, exposure of living samples to high intensity focused illumination can obscure the very processes we are trying to visualize. Minimization of the excitation-light dose is an effective approach to reduce photo toxicity. Nevertheless it reduces signal to noise (S/N) ratio, and diminishes image quality. Photo bleaching on the other hand is light-induced change in a chromophore, resulting in the loss of its absorption of light at the typical absorption band of the molecule[44].

This phenomenon is a common problem in fluorescence microscopy or in plate reader based analyses of cells. Hence finding a suitable balance between light exposure and cell viability is a continuous challenge in live cell interrogation[2].

Toward solving this problem a controlled light-exposure microscopy (CLEM) has been used. In CLEM, a non-uniform illumination of the fluorescent sample allows to adjust the light dose for the excitation of fluorophores for every individual pixel leading to reduced photo toxicity and photo bleaching without losing image quality. CLEM instrumentation is also simple. For

example to change an existing confocal microscope to CLEM-confocal, a fast shutter is placed in the laser beam in order to switch on and off the illumination light within the pixel dwell time. An electronic circuit, which functions as a fast feedback system, controls the shutter depending on signals from the detector and calculates signal for the formation of image[45].

Hoebe R.A. et.al used Controlled light-exposure microscopy (CLEM) to indirectly measure and reduce photo bleaching and photo toxicity in fluorescence live-cell imaging. According to this paper, bleach rates were reduced seven-fold by CLEM, and production of reactive oxygen species (ROS) in HeLa cells, expressing a GFP-tagged histone protein (H2B-GFP) loaded with a ROS indicator, was reduced eight-fold as compared with non-CLEM. An interesting conclusion that can be drawn from this finding is that incident light could have a large effect on live cells, particularly when observing ROS-depending process[45,46].

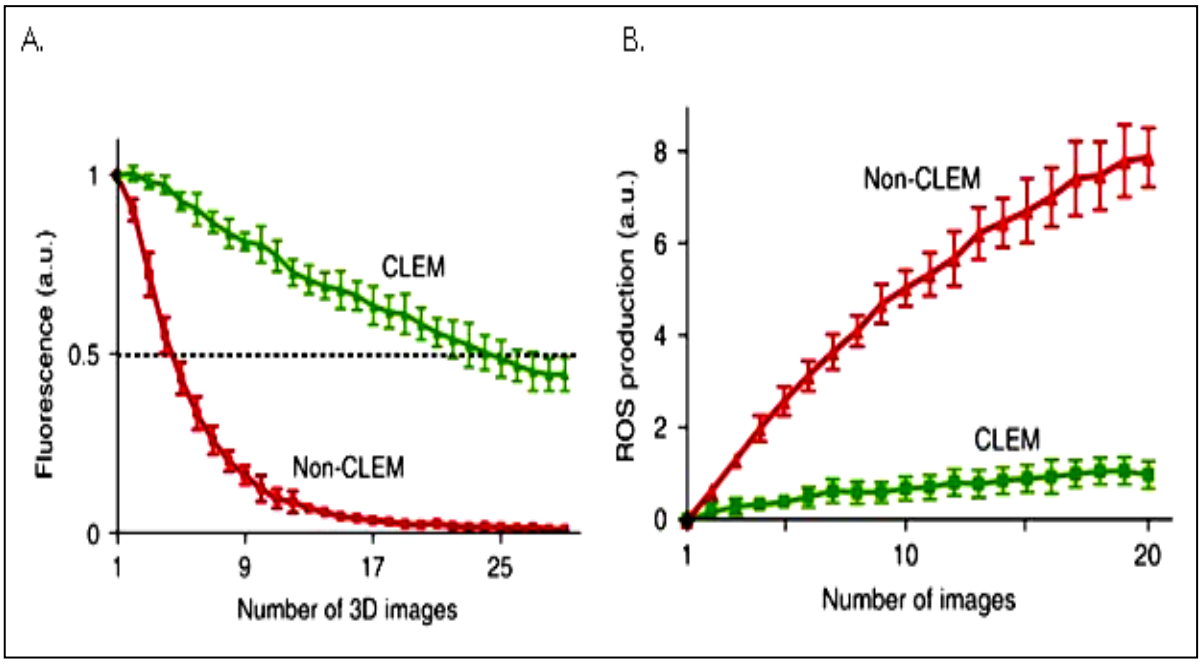

Fig.2.1 A) Analysis of photobleaching curves shows that bleach rate is sevenfold reduced by CLEM. a.u. (arbitrary units) B) Production of ROS in HeLa cells
From [45]

This technique gave much hope in live cell imaging, yet it only reduces photo bleaching, eventually ROSs will accumulate and impair the cell cycle. The best way to turn away from this problem would be to avoid direct exposure of live cells with the incident light. Towards this goal, we applied customized micro-wells made with 3D-printed templates to quantify free fatty acid uptake by adipocytes.

2.2 3D printing and 3D printed template interfacing

3D printing or additive manufacturing (AM), is the processes of creating three-dimensional objects. Digital models made with computer aided design (CAD) software are taken to 3D scanners. Slicer software is used to obtain a series of layers on Z- direction separate from the 3D models. Finally, a 3D object is made by layer by layer printing or superposition using powder, molten plastic, or metals to create the material scaffolding. Although still in development, 3D printing methods can roughly be classified as extrusion-based, photocuring, photo melting, inkjet-based and paper cutting. Jeremy Rifkin on 'the third industrial revolution' envisioned, as the new 3-D technology becomes more widespread, on site, just in time customized manufacturing of products will reduce logistics costs with the possibility of huge energy savings. Currently this technology is so rampant, that it finds application in apparel, automotive industry, construction, jewelry, medical devices, bio-printing, space engineering and many more[47,48]. After designing models with sketchUp software, we produce our 3D templates in-house using a MakerBot Replicator2® printer. It is an extrusion based printer which uses poly lactic acid (PLA) filament for printing.

In designing an assay system which excludes direct exposure of cells by excitation light we turned to 3D-printed interfacing systems previously developed in our lab. Several macro-to-micro interfacing3D-printed templates were used to bridge endocrine tissue and microfluidic

systems. These templates were found to be suitable in endocrine tissue secretion sampling[40]. Herein, we used similar templates to fabricate micro-well plates that reduce or illuminate exposure of cells to light in a plate reader instrument, while still permitting fatty acid uptake quantification.

2.3 Reagents and experimental methods

2.3.1 Reagents and chemicals

Insulin, D-glucose, 4-2-hydroxyethyl-1-piperazineethanesulfonicacid (HEPES), nystatin, fluorescein, KH2PO4, and NaH2PO4 were purchased from SigmaAldrich (St Louis, Missouri). Bovine serum albumin (BSA), fetal bovine serum (FBS), NaCl, $CaCl_2 \cdot 2H_2O$, and blunt ended needles were purchased from VWR (West Chester, Pennsylvania). Penicillin–streptomycin, Minimal Essential Media (MEM) non-essential amino acids solution 100×, sodium pyruvate, L-glutamine, and Dulbecco's Modified Eagle Medium (DMEM), $MgSO_4 \cdot 7H_2O$, and BODIPY FL C16 were purchased from ThermoFisher Scientific (Grand Island, New York). 3T3-L1 pre-adipocytes were purchased from American Type Culture Collection (ATCC ®) (Manassas, VA 20110 USA). PLA filament was purchased from Amazon.

2.3.2 3D template fabrication and characterization

A modification of micro-well architecture was required to block optical excitation of adipocytes while preserving interrogation of solution fluorescence. 3D-printed templates were used as molds for polydimethylsiloxane (PDMS) micro-wells, allowing rapid prototyping of various architectures. Optimized PDMS microplates included 24 wells (7.5 mm diameter) with tissue culture moats on well floors, 3D-printed caps (polylactic acid, or PLA) with 2-mm diameter pinholes, and a 3D-printed microplate base replica. These hybrid PDMS/PLA microplates allowed interrogation of the solution but prevented excitation of moat regions, which allowed

real-time quantification of FFA uptake dynamics, along with minimizing photo toxicity of the cells. A 3D replica of the commercial microplate with 24 wells (7.5 mm diameter) which include a 2mm high moat area was modelled in Sketchup© software (Trimble Navigation Limited) and printed with a Makerbot Replicator-2 using black polylactic acid filament (PLA, 1.75 mm diameter). 3D printed cover caps with 2-mm diameter pinholes were also made similarly. (Fig.2.2B)

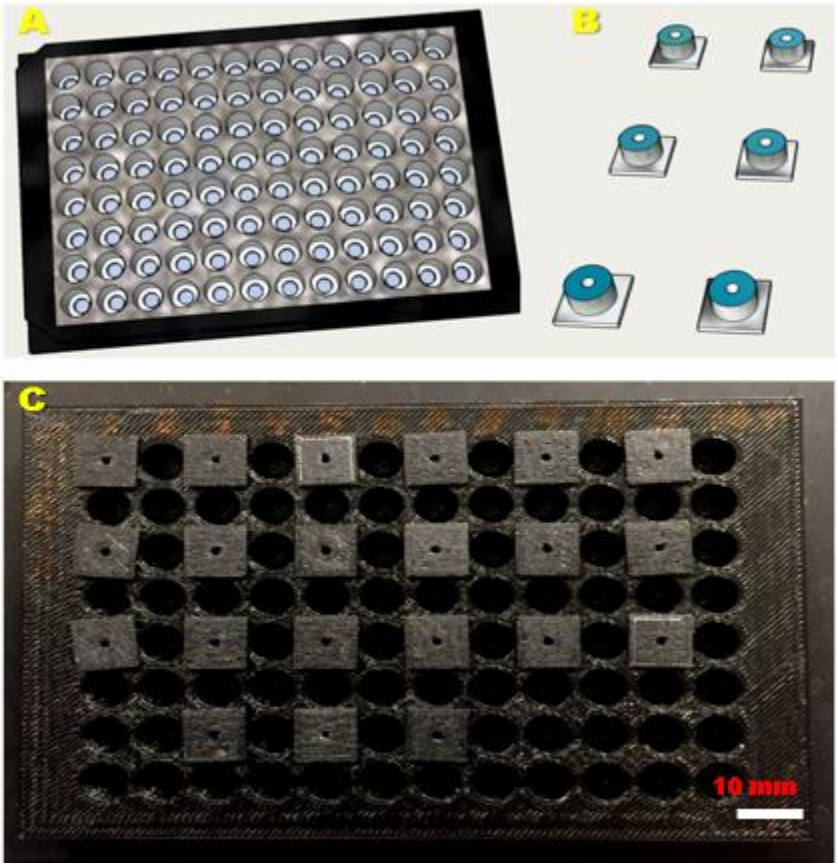

Fig. 2.2 A) Design of the commercial microplate replica prepared in sketchup B) Design of cover caps prepared in sketchup C) The actual 3D-printed microplate with some of its wells covered with the pinhole-containing 3D cover-caps.

2.3.3 3T3-L1 cells treatments and experimental result

3T3-L1 pre-adipocytes were grown in a 25 cm^2 flask following a previously developed protocol[49]. Cells were washed with saline solution and starved for two hours with DMEM (serum

and phenol red free) containing 3.5 nM and 50 pM glucose and insulin respectively. Subsequently media was removed and replaced with fresh 300 ml of fresh media.

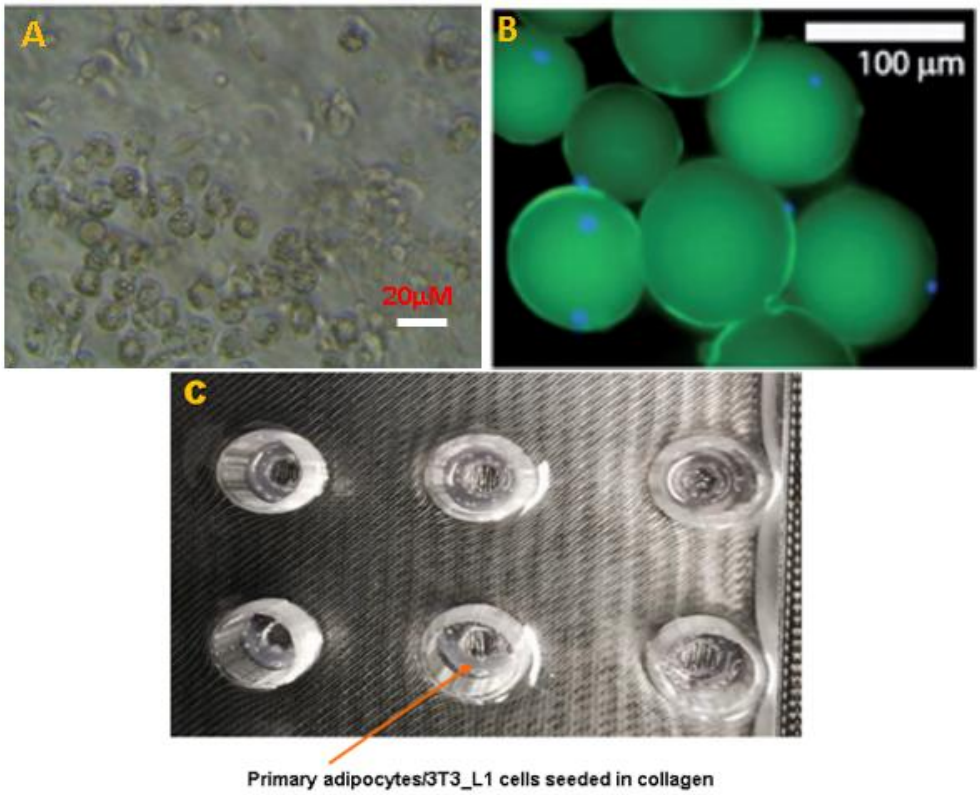

Fig.2.3 A) Diferentiated 3T3-L1 cells B) primary adipocytes, and C) adipocytes (primary and 3T3-L1 cells) seeded in collagen embedded around the moat area of our 3D-printed microplate

For securing cells at the bottom of the well, we use collagen in a 1:1 ratio with the cells. The mixture was then incubated for one hour at 37 °C. 100 µL was loaded in each well. After cells were fully attached to the bottom of chip surrounding the moat area, a 3D-printed cap with 2mm diameter pinhole was fixed to cover the area surrounding moat. 100 µL of 2.5 µM BODIPY FL C16 was then added at 0, 15, and 30 minutes. Fluorescence was read using a microplate reader immediately after the last loading step.

2.4 Results

2.4.1 Validation of free fatty acid uptake in a PDMS chip using standard 96-well microplate

The uptake kinetics of BODIPY FL C16 fluorescent fatty acids was initially validated as follows. Briefly primary adipocytes from mice were pre-treated with either high glucose/high insulin (HGHI; 11 mM glucose, 500 pM insulin) solution or low glucose/low insulin (LGLI; 3.5 mM glucose, 50 pM insulin) solution, and cells were incubated on PDMS device (chip) with 20 µM of labeled palmitic acid, BODIPY FL C16. Every 30 minutes, 2 µL aliquots were transferred to a 96-well plate which contained 48 µL of 1xHBSS buffer. Fluorescence was then measured using a Filter Max F5 multi-mode plate reader. Samples were run in triplicates.

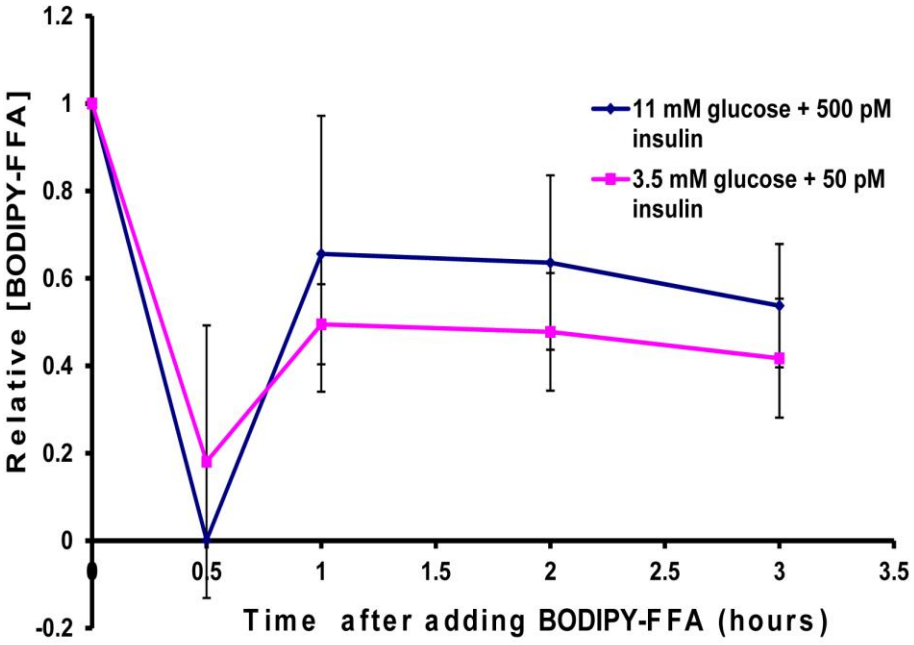

Fig.2.4 Relative BODIPY FL C16 (BODIPY-FFA) uptake Uptake kinetics after treating cells with LGLI (3.5 mM glucose, 50 pM insulin) (pink trace) or HGHI (11 mM glucose, 500 pM insulin)) (blue trace) treated mice

First, we confirmed that BODIPY-FFA uptake measurement could be achieved in primary adipocytes using manual pipetting and off-line measurement of fluorescence in a plate reader. In

Fig.2.4 above, fluorescence is given in relative units (RFU) normalized to initial fluorescence. Adipocytes on standard HGHI absorbed all the labelled fat (BODIPY FL C16 or BODIPY-FFA) in less than 30 minutes (blue trace) and those in LGLI took most of it (pink trace). Both the HGHI and LGLI treated adipocytes appeared to release more than half of the BODIPY-FFA in the next half hour. The uptake kinetics largely equilibrated within an hour. This uptake kinetics from manual pipetting of solutions incubated with primary murine adipocytes, and observation of a rapid uptake in <30 minutes confirmed that cellular mechanisms for FFA uptake were intact and functional, and some insulin dependence was observed. The dynamics agreed with work carried out by others[50].

However, to achieve a real-time FFA uptake assay, manual pipetting steps must be excluded and direct excitation of cells should be eliminated. Toward this goal, a modification of micro-well architecture was required to block optical excitation of adipocytes while preserving interrogation of solution fluorescence.

2.4.2 FFA uptake kinetics by 3T3-L1 Cells using a 3D-printed microplate

3T3-L1 adipocytes were grown in a 25cm^2 flasks. They were washed twice with saline solution and starved for 1 hour with DMEM containing LGLI solution (3.5 nM and 50 pM glucose and insulin). Media was removed and replaced with 300 ml of fresh media. For securing cells at the bottom of the well, collagen in a 1:1 ratio with the cells was used, in preparation for a three-dimensional culture in collagen matrix.

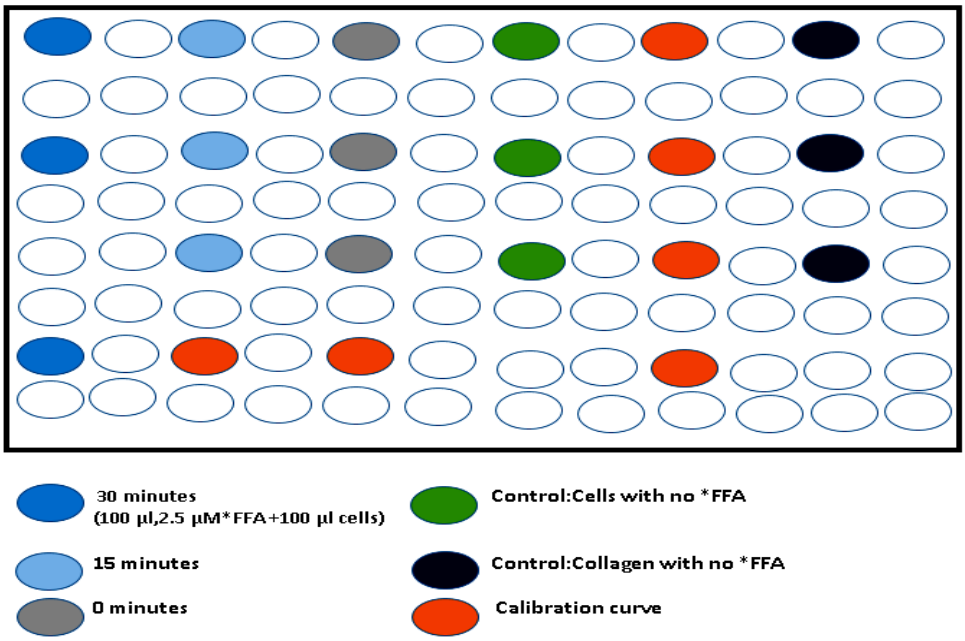

Fig.2.5 Schematic of the arrangement of wells in the 3D-printed Microplate

The mixiture was then incubated for one hour at 37 °C.100 µL of the cell/collagen mixture was loaded into each well (**Fig. 2.5**). After cells were fully attached to the bottom of the microplate, a 3D-printed cap with 2-mm diameter pinhole was attached above the well. Finally 100 µL of 2.5 µM BODIPY-FFA in HGHI (with 500 pM Insulin and 11 mM glucose) was pipetted at 0, 15, and 30 minutes. After the final loading, fluorescence was read immediately using a microplate reader.

Fig.2.6 shows uptake analysis of this experiment for a total of 30 minutes. 3T3-L1 cells did not take any BODIPY-FFA until after the 15 minute time point, but uptake was abrubt in the next 15 minutes. As shown by the graph, cells took almost all of the BODIPY-FFA after 30 minutes. Compared to our previous results with primary adipocytes, this result from 3T3-L1 cells uptake was more gradual. This could signal inherent differences in uptake metabolism between primary and 3T3-L1 adipocytes, or there could simply be a difference in cell density within the microwell. The fairly large error bars are atributed to the fact that 3D-printing using PLA results

in a very slightly bulged sides in the microplate, which in turn results in slight difference in moat area exposed to exciting light and hence fluorescence intensity (RFU) between replicate wells. Assuming a perfectly stright microplate, which can be achieved using strong material (like steel or more rigid plastics) for 3D-printing, the above problems should be adressable.

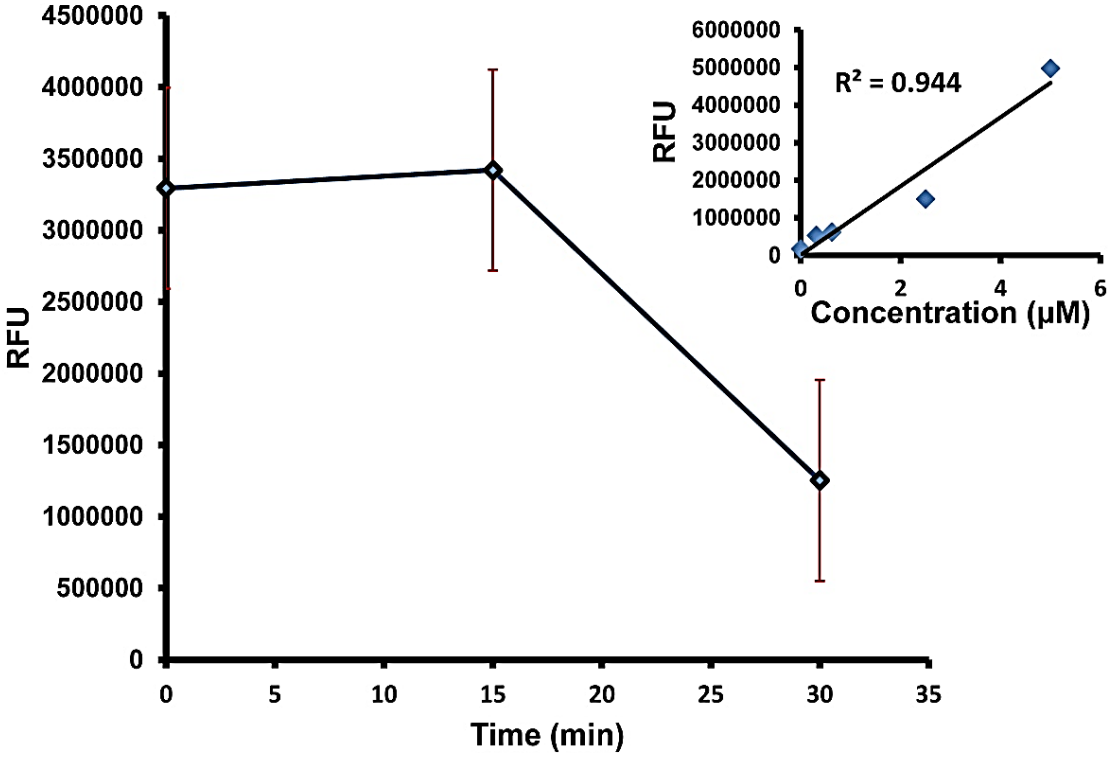

Fig.2.6 Uptake kinetics of 3T3-L1 during 30 minute time; Insert represents the Calibration curve

2.4.3 Labeled free fatty acid (BODIPY C12) uptake: A titrimetric experiment

From our previous observations we understand that explants (3mm diameter in this case) likely reach a saturation level during BODIPY-FFA uptake. In this experiment, we aimed at determining an average saturation point for a given explant tissue volume by gradually titrating the tissue with BODIPY-FFA until cellular uptake was no longer possible. These results will be useful for a variety of future experiments involving BODIPY-FFA uptake kinetics in microfluidic systems.

Six 3-mm diameter explants (wet volume) were incubated with 100 µL DMEM in micro centrifuge tubes separately. The first three explants were treated with 100 µL HGHI (20 mM / 10 nM) in DMEM. We treated the next group (three explants) with 100 µL of LGLI (5.5 mM / 50 pM) in DMEM. 20 µL of 3 µM BODIPY-FFA (BODIPY C12, in this case) was added and mixed by pipetting [final concentration=0.5 µM]. After 10 minutes, 20 µL from each explant was transferred to a microplate well, preloaded with 60 µL of DMEM (which make up the volume suitable to read using microplate reader). Every 10 minutes we continued to add 20 µL of 3µM BODIPY-FFA, while after mixing by pipetting, 20 µL was transferred to the microplate for readout (zero net change in volume). After the fifth addition (50 minute time point and final solution concentration of 1.79 µM) we measured the fluorescence using a microplate reader. We used buffer solution (DMEM with high/low glucose and insulin) as our control.

In **Fig.2.7A**, we observe the average fluorescence (RFU) of three explants under high glucose/insulin (blue trace) and those under low glucose/insulin (orange trace) gradually returning to match with the control group. This indicates that explants were constantly taking-in BODIPY-FFA while its concentration increases from 0.5 µM to around 1.55 µM. After titrating to the final concentration of 1.79 µM explants in both treatments were unable to uptake more BODIPY-FFA. This can be seen by the explant fluorescence traces matching with corresponding trace from the control group (black trace).

The difference in counts (fluorescence intensity in RFU) between explants and control, versus time (Fig.2.7B) gives a clear indication that the explants were saturated with BODIPY-FFA.

This data set can be simply converted to the amount of BODIPY-FFA stored by each explant over time (in units of pmole), as shown in **Fig.2.7C**.

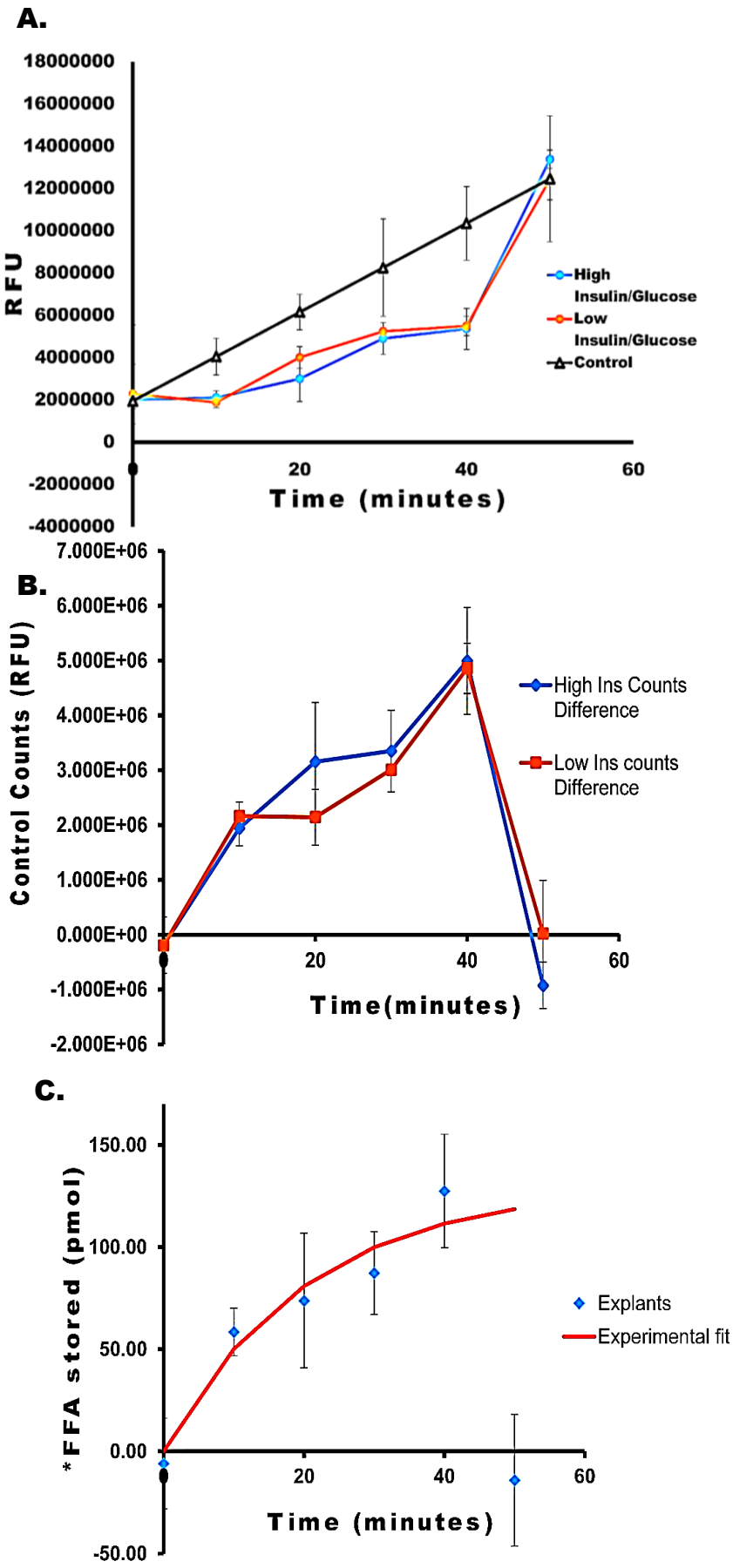

Fig.2.7 A) BODIPY-FFA (BODIPY C12) uptake kinetics of six (6) explants (3 with High Insulin/Glucose + 3 with Low Insulin/Glucose)
B) Difference in Counts (RFU) for High/Low Insulin/Glucose treated explants and the control
C) BODIPY-FFA stored during measurement time

2.5 Discussion and Conclusion

In the past few years, a variety of assays has been developed by our Lab which targets endocrine secretions[51,40,39]. As mentioned above, many techniques have also been used by other groups to this end, but are limited by cost, safety, and need of special training. Initially our goal was to develop a simple, fluorescence-based method for quantitative FFA uptake without the disadvantage of phototoxicity. As discussed in Chapter 1 and in this chapter, we applied a modification of micro-well architecture to block optical excitation of adipocytes while preserving interrogation of solution fluorescence. Microplates included 2-mm height moats on well floors and 3D-printed caps (polylactic acid, or PLA) with 2-mm diameter pinholes. The pinholes allowed interrogation of the solution but prevented excitation of cell moat regions, which allowed real-time quantification of FFA uptake dynamics, along with minimizing phototoxicity to cells. The characteristic warping at the edges that typically emerge in 3D-printing using poly lactic acid (PLA) is the main limitation, which caused reasonable error between measurements. Nevertheless, we believe it is promising approach that could be improved with a better material for printing (like steel) or a higher resolution printer. The system is also well-poised for future integration with microfluidic channels. In the next chapter, we will discuss our microfluidic approach to quantitative free fatty acid uptake in adipocyte tissue explants, which exhibits a number of advantages compared to the microplate format.

For the explant titrimetric experiment, in the first 10 minutes explants absorbed nearly half of the BODIPY-FFA (BODIPY C12) from the solution. They continued to absorb slightly more up to the 40 minutes time point (Final solution concentration=1.55 μM), at which point they completely stopped BODIPY-FFA uptake. The data indicate that the explants reached saturation at this concentration, which translates to 130×10^{-12} moles (130 pmol) of BODIPY-FFA taken

up in the average explant (n=6). Interestingly, we did not observe an appreciable difference in uptake amount between our high and low glucose and insulin treatments in this experiment. Nonetheless, this information is novel and particularly useful for other experiments in the Easley laboratory involving explants.

With a few approximations, this data can be used to determine the amount of BODIPY-FFA uptake that should be expected per adipocyte. Considering that the explants were 3 mm in diameter and about 0.3 mm in height, the explant volume is 2.12 μL. Using an average cell diameter of 50 μm (volume = 6.54×10^{-5} μL), this explant volume translates to about 32,400 cells per explant. Using our determined value of 130 pmol BODIPY-FFA absorbed per explant (**Fig.2.7C**), we can estimate that each normally functioning adipocyte can take up approximately 4.0×10^{-15} mol BODIPY-FFA (~4 fmol/cell). These data are very well correlated with other measurements in our laboratory (data not shown) using 3T3-L1 adipocytes, where it was determined that BODIPY-FFA is taken up at a rate of $3.5 \pm 0.2 \times 10^{-15}$ mol $cell^{-1}$.

CHAPTER 3

Development of real-time, quantitative free fatty acid uptake assays for adipocyte tissue explants using microfluidics

3.1 Introduction

3.1.1 Improving Methods for Fatty Acid Uptake Analysis

Recently adipose tissue has been identified as a critical endocrine organ which secretes various hormones and peptides (adipokines) including leptin, adiponectin, adipolin, visfatin, omentin, tumour necrosis factor-alpha (TNF-α), interleukin-6 (IL-6), resistin, pigment epithelium-derived factor (PEDF), and progranulin (PGRN) which dramatically influence insulin sensitivity[52,53,54].

In addition, asprocin is a recently discovered adipokine with profound effects on gluconeogenesis in the liver[55]. One of the major hormones effecting adipose tissue is insulin. Elevated insulin stimulates fatty acid uptake, and prolonged excessive uptake of free fatty acids has been linked to insulin resistance and adipose tissue hypertrophy which ultimately leads to obesity and other chronic diseases[42,56].

As noted in chapter 1, available quantification techniques for FFA uptake have many limitations; the use of radioactive compounds, the need for micro injection of cells and the failer to address the complex uptake mechanisms are some of the problems. Furthermore, the lack of dynamic information with many of the current techniques is a significant problem that limits our understanding of this tissue. For this reason, developing improved methods for measuring FFA uptake dynamics is very important and highly needed to enhance our understanding of disease states such as obesity and diabetes. For this project, we decide to employ a microfluidic technique which is simple and readily available in our laboratory to address the aforementioned

needs. Our method combines a microfluidic chip with standard fluorescence microscopy, which makes it instrumentally simple and cost effective. Our system also allows us to continuously flow our reagent to surround the tissue explants to better imitate the physiological environment. This chapter will describe the approaches used to implement our microfluidic analysis method, and herein we will present proof-of-concept that the system is capable of collecting novel, dynamic information about adipose tissue function.

3.1.2 Microfluidics

Microfluidics is the science that studies flow of liquids inside micrometer-sized channels, typically tens of micrometer (μm) scale. It is a multidisciplinary field intersecting engineering, physics, chemistry, biochemistry, nanotechnology, and biotechnology. Typical liquid volume is in the nanoliter range. Such dimensions are useful to exploit liquid properties which govern at this scale. If the dimension of a system is characterized by length scale L, area scales as L^2 and volume scales as L^3. The surface properties (like capillary force) are in general proportional to the surface area and volume properties (like weight) are proportional to the volume. The surface-to-volume ratio scales as L^{-1}. This ratio increases when changing from macroscopic to microscopic systems. In microsystems surface forces tend to dominate over volume forces. The capillary and interface phenomena become dominant whereas gravity and inertia become less important. Consequently, surface effects which are insignificant in large-scale fluidic manipulation become important at the microscale. Flow inside microfluidic channels is laminar and turbulence does not occur because Reynolds number, Re, and characteristic fluid velocity, μ, have a very low values. Reynolds number, Re, is a dimensionless parameter defined as $Re = \rho L\mu/\dot{\eta}$, i.e. the ratio of inertial to viscous force on fluid, where ρ and $\dot{\eta}$ are the density and the viscosity of the fluid respectively. Owing to above mentioned characteristics many micro-

devices are being developed for various purposes that exploit unique physical properties at this scale [57,58].

The Kennedy group pioneered monitoring secretion of hormones and fatty acids from adipocytes, particularly murine 3T3-L1 adipocytes using microfluidics. Their device incorporated a cell perfusion chamber and an analysis section. Cells were interrogated under buffer followed by isoproterenol to induce lipolysis conditions. They were able to assay glycerol and fatty acids with a limit of detection (LOD) of 4μM and 5μM respectively[59].

The same group developed another chip capable of sequential electrophoresis-based immunoassays on other endocrine tissues by multiplexing microfluidic channels. In this chip, insulin-containing perfusate from islets of Langerhans is fed in to a reaction chamber by electrophoresis and mixed with fluorescein isothiocyanate-labeled insulin (FITC-insulin) and anti-insulin antibodies. Secretion is monitored and detected using laser-induced fluorescence technique[60].

Evaluation of active insulin secretion from both human and mouse islets using microfluidic perfusion devices have also been reported. A microfluidic device to perfuse pancreatic islets with a simultaneous description of their functionality through fluorescence imaging of the mitochondrial membrane potential and intracellular calcium ([Ca2+]i).it was considered a gold standard to predict islet functionality prior to transplantation[61,62].

In a novel approach developed by our lab, a microfluidic chip that integrates a customized primary tissue culture reservoir into a passively operated microfluidic device made of polydimethylsiloxane (PDMS) was used to culture and sample adiponectin from primary adipocytes. This technique introduces new methods for sculpting the above-channel PDMS

substrate. In addition the design permitted 3D culturing which better mimics in-vivo architecture of adipose tissue[51].

Microfluidics also allows automation and multiplexing of laboratory techniques. Efficient consumption of reagents, high-throughput analyses, miniaturized components, and low cost of production makes it an appealing technology. It has found application in many areas in academic research, although its commercial application so far is mainly in genomics and point of care diagnostics[63].

3.1.3 Fluorescence Microscopy

Fluorescence is the luminescent emission that results from absorption of photons. Phosphorescence, on the other hand, is the longer-lasting "afterglow" counterpart of fluorescence. They differ by the magnitude of the decay time. Fluorescence emission ceases abruptly when the exciting energy is shut off. The decay time, of the emission is on the order of 10^{-8} sec and results in a negative frequency-shifted emission. Phosphorescence decay takes place in milliseconds to seconds. The fluorescent effect is particularly useful for fluorescence microscopy for biological applications. The principal use of fluorescence microscopy is to examine specimens that have been treated with special fluorescent reagents (BODIPY FL C16 and BODIPY®558/568 C12 in our case). BODIPY FL C16 is able to absorb light over a band centered at 505 nm wavelengths and emit light with a 510 nm wavelength maximum, shifted toward the red end of the spectrum from the absorbed light due to the classic Stokes shift.

As discussed in detail in this chapter, fluorescence microscopy allows us to selectively examine the BODIPY labelled FFA in the solution from the channel with tissue explant at the targeted area downstream. At this area, all the channels are in parallel, and imaging with a CCD camera allows discrimination between multiple samples at once and in real-time. In this way, we exploit

the benefits of both microfluidics and fluorescence microscopy to develop novel methodology for real-time, quantitative fatty acid uptake analysis from adipose tissue[36, 66].

3.2 Reagents and Experimental methods

3.2.1 Reagents and Chemicals

BODIPY®558/568 C12-(4, 4-Difluoro-5-(2-Thienyl)-4-Bora-3a,4a-Diaza-s-Indacene-3-Dodecanoic Acid) and BODIPY FL C16 were purchased from ThermoFisher Scientific (Grand Island, New York). Insulin, D-glucose, 4-2-hydroxyethyl-1-piperazineethanesulfonicacid (HEPES), nystatin, fluorescein, KH_2PO4, and NaH2PO4 were purchased from SigmaAldrich (St Louis, Missouri). Bovine serum albumin (BSA), fetal bovine serum (FBS), NaCl, $CaC_{l2}\cdot 2H_2O$, and blunt ended needles were purchased from VWR (West Chester, Pennsylvania). Penicillin–streptomycin, Minimal Essential Media (MEM) non-essential amino acids solution 100×, sodium pyruvate, L-glutamine, and Dulbecco's Modified Eagle Medium (DMEM), $MgSO_4\cdot 7H_2O$, was purchased from ThermoFisher Scientific (Grand Island, New York). Polydimethylsiloxane (PDMS) precursors, Sylgard® 184 elastomer base and curing agent, were obtained from Dow Corning (Midland, Maryland, USA). Silicon wafers were obtained from Silicon, Inc. (Boise, ID, USA), SU-8 photoresist and developer were purchased from Microchem (Newton, Massachusetts, USA), Tubing for interfacing syringes and devices was obtained from Small Parts (TGY-020-5C; 0.02 in. ID, 0.06 in. OD, 0.02 in. wall). Male C57BL/6J mice were purchases from Jackson Laboratories. All experiments involving animals were performed in compliance with relevant laws and institutional guidelines and were approved under protocol number 2014-2096 by the institutional animal care and use committee (IACUC) of Auburn University.

3.2.2 Harvesting adipocyte tissue explants

Our laboratory utilizes protocols for harvesting primary adipocytes from mice. Researchers in various disciplines (especially in biology and medicine) have been using primary adipocytes or fully differentiated 3T3-L1 cells for various experiments. In order to maintain adipose tissue homeostasis and limit harsh treatments leading to primary adipocytes, we have recently started using intact tissue explants for our analysis. Adipocyte explants are harvested as previously described[64,49,40]. Briefly, the mouse is anaesthetized using a Ketamine/Xylazine mixture (~0.1-0.15ml for lean mice and 0.2-0.25ml for overweight mice) by injecting intraperitoneally. V-shaped cut is made by grasping the mouse just below the metasternum with small forceps and the stomach is sliced open with scissors. Fat pads are then cut and collected. Further explants of ~3mm diameter (wet volume) are excised from the tissue using a 3-mm biopsy punch. Explants are incubated in 5% CO_2 with DMEM. Media is replaced every day; uptake studies were done either on the day of harvesting or within 3 days.

3.2.3 3D printed template fabrication

The 3D structure of a convenient interface templates were fabricated in-house using appropriate 3D CAD software (e.g. SketchUp, OpenSCAD). Templates and parts presented in this thesis were printed using a MakerBot Replicator 2 with PLA filament. Sample print of these templates is shown in **Figure 3.11C**. After rinsing the silicon wafer with methanol and dried with N2 gas, an aluminum foil folded in a cylindrical shape is used to hold the wafer. Wafer is gently pushed flat onto the bottom of the foil. Previously degassed PDMS was slowly poured on top of the wafer. Interface templates are placed over the appropriate structures in the PDMS to define the reservoir regions above channel designs (see **Figure 3.11.A**) and the whole structure (wafer,

templates, and PDMS) is degassed to remove any trapped between the wafer and the template. Finally it is gently adjusted and placed in an oven to cure the polymer.

3.2.4 Microfluidic chip Fabrication

We used standard soft lithography techniques to fabricate polydimethylsiloxane (PDMS) microchips as described elsewhere[65]. Designs of networks of channels were first generated by a computer drawing in Adobe Illustrator software and printed as photomasks at 50800 dpi resolution by Fineline Imaging (Colorado Springs, CO). PDMS elastomer base and curing agent were mixed in a 10:1 ratio, then poured over the master defined by photoresist (SU-8, Microchem) on a silicon wafer. A custom made 3D-printed template was placed into the uncured PDMS which served as a macro-to-micro interface. The interface contained a tiny foot, inside which the explants were trapped (Refer **Fig.3.11A, red rectangle**).

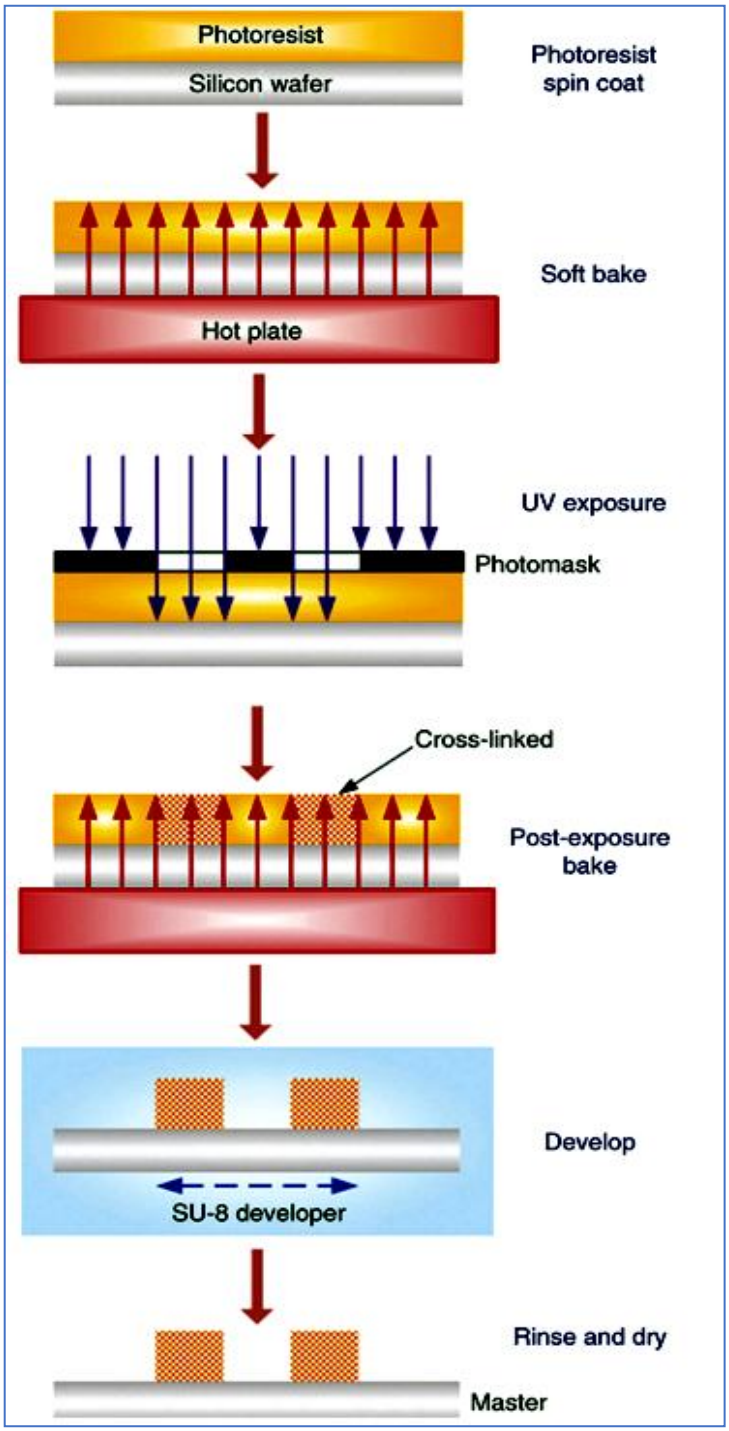

Fig.3.1 Schematic illustration of master fabrication with standard photolithography technique
From [65]

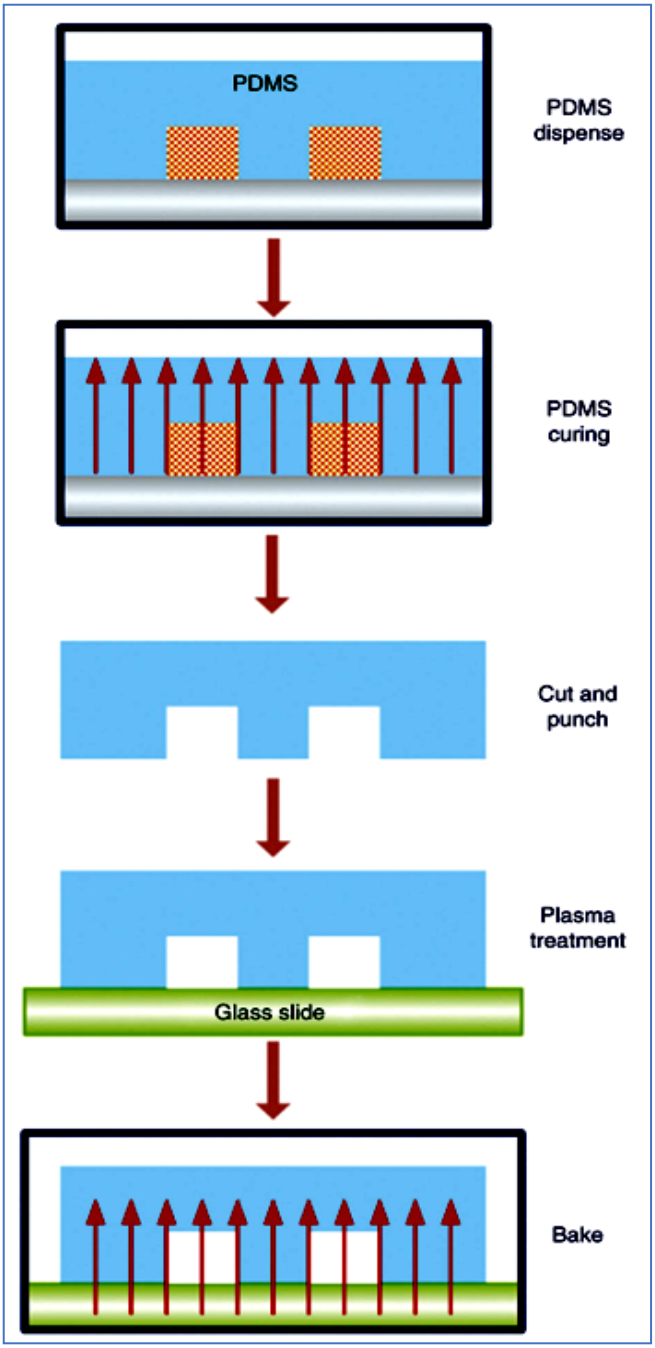

Fig.3.2 Schematic illustrations of PDMS device fabrication- using the silicon-wafer master From [65]

PDMS was cured at 65 °C for 2.5 h. Finally patterned PDMS are peeled from the silicon wafer and diced into individual devices.

An in-house fabricated CO_2-laser was used to drill a hole through the foot to connect to the micro channels (**Fig.3.11B**). The wafer was then cleaned with methanol, air-dried with a nitrogen stream, and immediately bonded to glass slides exposed to air plasma for 45 s (Harrick Plasma). Prior to use micro-channels were treated with DMEM cell-culture media containing 0.2% Bovine Serum Albumin (BSA) for one hour. The treatment with BSA is critical, because the labelled fatty acids are easily absorbed by the PDMS walls which can interfere with analysis. To control flow in the microfluidic device, a home-made manifold connected with the devices via 0.02 in. ID Tygon tubing (Small Parts) was used. Vacuum was applied using a hand-held, 100-mL syringe (SGE Analytical Science).

3.2.5 Fluorescence Microscopy and Data Analysis

Fluorescence imaging and measurements in our device were done with a cooled CCD camera (CoolSnap HQ2; Photometrics Scientific) interfaced to a Nikon Ti-E inverted fluorescence microscope operating in wide-field transmittance mode. Dual band excitation and emission, isothiocyanate (FITC) and tetramethylrhodamine isothiocyanate (TRITC), filter cube was used for detection of BODIPY FL C16 (excitation: 470 ± 20 nm; emission: 525 ± 25 nm) and BODIPY C12 (excitation: 559 ± 3 nm; emission: 568 ± 4 nm). Images were captured at 20 × magnification, 1 image every 10s for 30 min and saved in tagged image file. ImageJ was used for analysis. Simultaneously Images were captured from three calibration channels (with 10 µM, 5 µM and 2.5 µM BODIPY FL C16 or 1 µM, 0.5 µM and 0.25 µM BODIPY C12) continuously throughout the experiment time and analyzed. Finally, calibrated concentrations (in units of µM) were converted to uptake rates (in units of mol min^{-1}) after multiplying by the imposed flow rate.

3.3 Results and Discussion

3.3.1 Vacuum manifold fabrication

To apply a uniform vacuum to all five channels simultaneously, a manifold was fabricated in-house (Fig.3.3). A rectangular PDMS piece with 70 mm thickness was cut out from a 2.5 cm wide, 7.5 cm long rectangular PDMS. On either side of the larger rectangle, five 1 mm wide holes were punched through the sides to the open area. Tygon tubing (0.21 mm ID) was connected by inserting into the punched holes. Two microscope slides were plasma oxidized and sealed on both sides of the PDMS. To make an air-tight seal the manifold was soaked in fresh PDMS and baked. Finally, the manifold could be interfaced to a microfluidic chip.

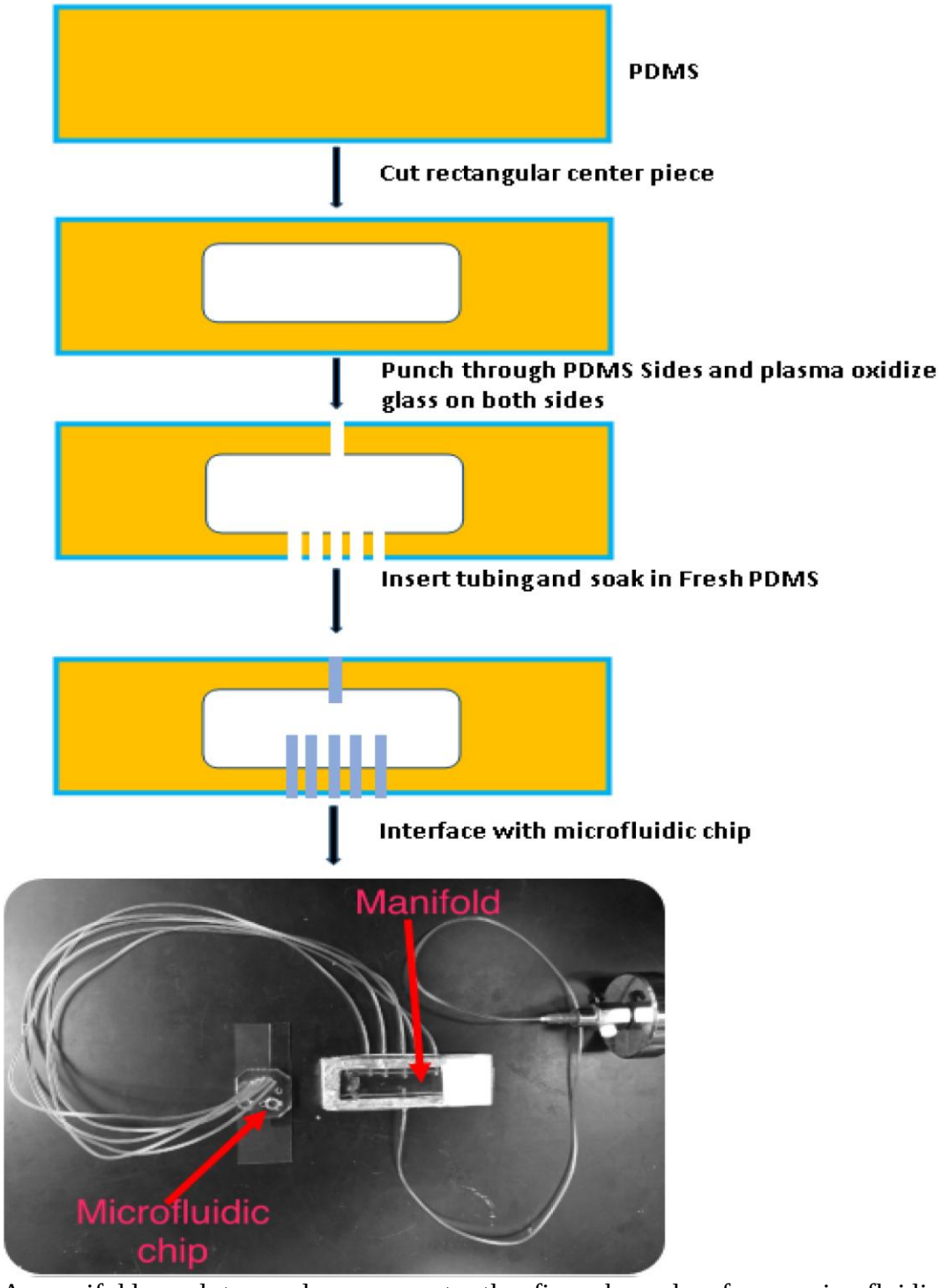

Fig.3.3 A manifold used to apply vacuum to the five channels of our microfluidic chip simultaneously.

3.3.2 Flow rate measurement

A constant flow rate throughout the measurement time is vital in continuous-flow analysis systems. We used our in-house made microfluidic manifold to help as achieve a steady flow rate. To calculated flow rate we measured the distance travelled by our reagent every 10 minutes after we applied vacuum through three different sized syringes; a 100-mL, 60-mL or 25-mL syringes. The internal diameter of tygon tubing is 0.5 mm. The calculated volume of manifold was 4.25 mL. The length of a single piece of tubing used was 25 cm and its total volume was determined to be 0.05 mL. The total volume of air which needed to be displaced was 0.3 mL (6*volume of 1 piece of tubing). Furthermore the total volume which needed to be displaced in the first vaccum application was ˜4.5 mL (manifold volume + Total tubing volume). After displacing the air vacuum was pulled to start the flow. With all syringes, a 1-mL volume displacement was used to induce flow. We calculated the volumetric flow rate (Q) (in µL/min) using the formulae below. Finally, we averaged the flow rates of the five tubings, and we used the 100 mL syringe for all of our additional experiments, the calculated flow rate of which was 0.55 µL/min.

$$\text{Volume Flow Rate (Q)} = \frac{A^* S}{\text{Time}}$$

A= Area
S= Distance travelled by reagent

Table 1: 25 mL syringe

Run	Time (min)	Distance (mm)					Volume (mm^3)					Volume flow rate (Q) (µL/min)				
		A	B	C	D	E	A	B	C	D	E	A	B	C	D	E
1	10	98	87	87	96	110	19.21	17.05	17.05	18.82	21.56	1.92	1.71	1.71	1.88	2.16
2	20	92	79	80	85	100	18.03	15.49	15.68	16.66	19.6	1.8	1.55	1.57	1.66	1.96
3	30															
Average (individual volume flow rate)												1.86	1.63	1.64	1.77	2.06
Average (overall) (µL/min)																**1.79**

Table 2: 60 mL syringe

Run	Time (min)	Distance (mm)					Volume (mm^3)					Volume flow rate (Q)				
		A	**B**	**C**	**D**	**E**	**A**	**B**	**C**	**D**	**E**	**A**	**B**	**C**	**D**	**E**
1	10	46	36	42	42	48	9.02	7.06	8.23	8.23	9.41	0.9	0.71	0.82	0.82	0.94
2	20	47	33	42	39	52	9.21	6.47	8.23	7.64	10.2	0.92	0.65	0.82	0.76	1.02
3	30	47	33	42	42	51	9.21	6.47	8.23	8.23	10	0.92	0.65	0.82	0.82	1.0
4	40	45	32	41	41	50	8.82	6.27	8.04	8.04	9.8	0.88	0.63	0.80	0.80	0.98
Average (individual volume flow rate)												0.91	0.66	0.82	0.8	0.98
Average (overall) (µL/min)																**0.83**

Table 3: 100 mL syringe

Run	Time (min)	Distance (mm)					Volume (mm^3)					Volume flow rate (Q)				
		A	**B**	**C**	**D**	**E**	**A**	**B**	**C**	**D**	**E**	**A**	**B**	**C**	**D**	**E**
1	10	29	25	32	32	36	5.69	4.9	6.27	6.27	7.06	0.57	0.49	0.63	0.63	0.71
2	20	15	22	31	32	40	2.94	4.31	6.08	6.27	7.84	0.29	0.43	0.61	0.63	0.78
3	30	10	20	35	32	40	1.96	3.92	6.86	6.27	7.84	0.2	0.4	0.69	0.63	0.78
4	40	9	16	33	30	34	1.76	3.14	6.47	5.9	6.66	0.18	0.31	0.65	0.59	0.67
Average (individual volume flow rate)												0.31	0.41	0.65	0.62	0.74
Average (overall) (µL/min)																**0.55**

The vacuum pressure of each system (P_ system) was calculated as follows,

$$P\_\ system = \frac{P\ (atmospheric)\ *Start\ Volume}{Ending\ Volume}$$

The volumetric flow rate (Q) and vacuum pressure difference in each system was found to be highly correlated, as can be seen from **Fig.3.4** below.

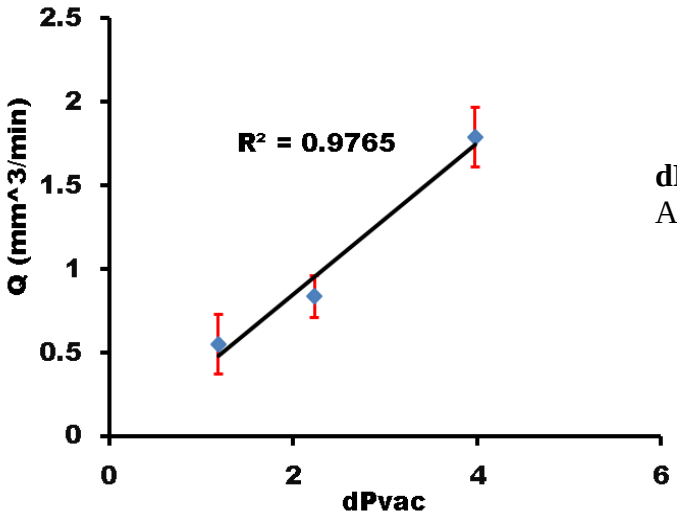

dPvac (vacuum pressure difference) = Atmospheric pressure – system pressure

Fig.3.4 Dependence of volumetric flow rate on vacuum pressure

3.3.3 The concept of continuous calibration by multi-channel imaging

Continuous fluorescence monitoring can be used to analyze dynamic behavior of cells, even facilitating real-time analysis of complex functions such as protein trafficking and protein-protein interactions. However, without customized ratiometric probes, this type of analysis usually provides only a qualitative view. For quantitative fluorescence analysis, microfluidic sampling provides a useful approach, yet drifts in the optical system and photodetector responses can result in poor reproducibility and sensitivity. Optical drift is an axial fluctuation which occurs because of gradual changes in focusing of sample and can result in skewed results if not accounted for. Here, we have devised a continuous calibration method for real-time, quantitative analysis of free fatty acids (FFA) in microfluidic channels downstream of cells. FFA quantities are determined, and signal drifts are corrected in real-time by imaging parallel calibration channels adjacent to adipose tissue sampling channels.

With the ultimate goal being real-time fatty acid uptake quantification in adipocytes, the desired method is to measure the sample and reference solutions in parallel. This can be afforded by

combining microfluidics with fluorescence microscopy. By positioning multiple parallel sampling micro-channels within the field of view of the microscope objective, as we will show later in this chapter, we can continuously quantify the leftover fluorescence in the perfused solutions compared to the reference solutions. This way, drifts in the microscope optics or 1/f noise at the detector can be largely corrected by constant referencing. This concept is nicely illustrated by calibration data which is collected in our optimized device design (see **section 3.3.6**), as shown in **Fig. 3.5**. This device was characterized using freely flowing fluorescein solutions at concentrations of 1.0 µM, 0.50 µM, and 0.25 µM. During a 30-min time period, typical cell sampling flow rates were induced, and fluorescence imaging of the 3 parallel channels was carried out at 0.1 Hz (one image every 10 s). A calibration curve could then be generated every 10 s for the 30-min period (180 calibration curves), and parameters such as slope, y-intercept, and R^2 could be determined in real time. **Fig. 3.5A** shows the fluorescence intensities from each of the 3 calibration channels. Optical system or detector drift was observed as slight increases in signal from about the 8-min time point to the 25-min time point, and this drift was present in all calibration solutions. With continuous calibration, it was possible to plot the slope, y-intercept, and R^2 values in real-time (**Fig. 3.5B**). The background drift was manifested by variations in the continuous trace in **Fig. 3.5B** depicting the slope (top trace), thus any calibrated data (shown later) will be effectively corrected for these background signal drifts. Note also that the y-intercepts were maintained at a level very close to zero (**Fig. 3.5B**, middle), and R^2 values were steadily hovering near 1.00 (**Fig. 3.5B**, bottom), as expected for a fluorescence signal on dark background with a good quality calibration. The multi-channel, real-time imaging of calibration solutions in a microfluidic format thus allows continuous quantification, noise correction, and continuous monitoring of the calibration quality. Use of this

method for labeled fatty acid uptake quantification ensures that we can confidently assign dynamic signal changes to the adipose tissue function and greatly reduce the possibility of false observations. As shown below, adipose explants exhibited insulin-dependent uptake of BODIPY-FFA, and dynamic information was collected in a manner that is not possible with end-point techniques, such as with fluorescence microplate readers. The passive operation of the presented microfluidic device provides ease-of-use[51], although this multi-channel imaging technique for real-time calibration and drift correction should also prove useful in future devices using active valving.

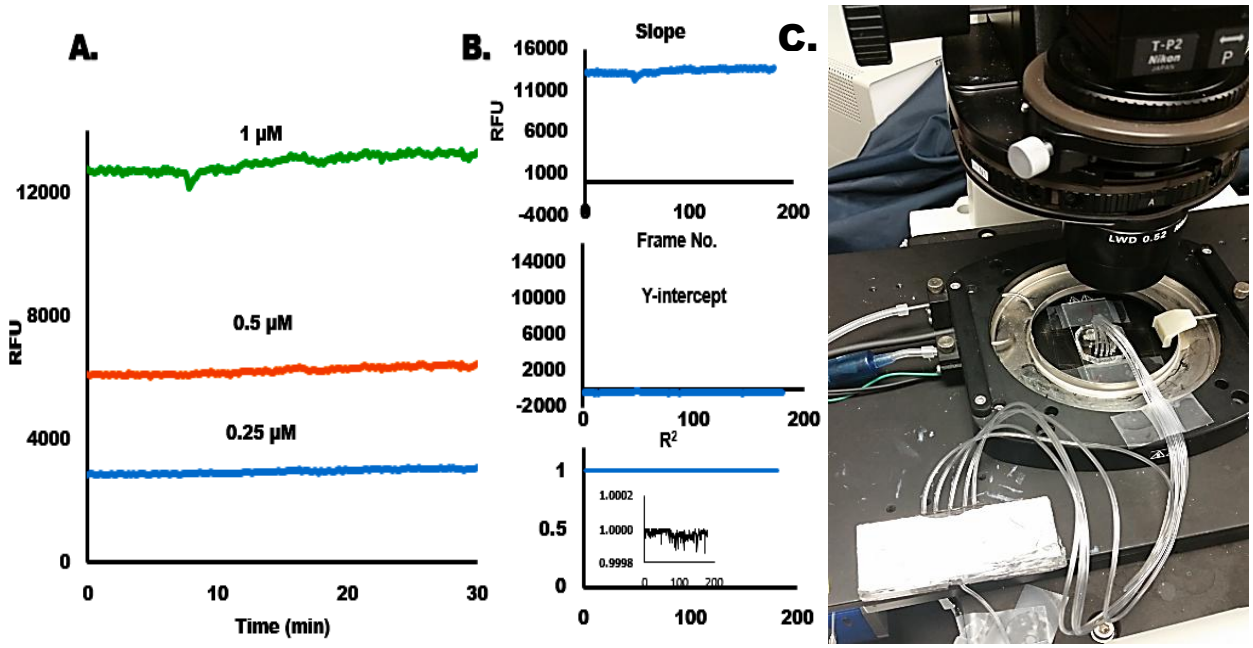

Fig.3.5 Continuous calibration by multi-channel imaging A) Fluorescence traces from calibration channels with 1.0, 0.50, and 0.25 µM fluorescein. B) Calculated continuous traces depicting slope, y-intercept, and coefficient of determination (R^2) throughout the measurement time can be used to correct for background drifts and monitor calibration quality C) Microfluidic chip on microscope stage ready for uptake measurement

3.3.4 Uptake kinetics of BODIPY FL C16 using the first generation multi- channel microfluidic chip

As mentioned above fatty acid with 16-carbon atoms which is classified as very long chain fatty acid has been used by others in applications regarding uptake and imaging, but uptake kinetics

have yet to be extensively studied. We started our experiment with BODIPY FL C16. As a first-generation device we initially used a seven channel microfluidic layout, which had been previously designed as a versatile device for parallel fluorescence measurements by microscopy. 2-mm diameter adipose tissue explants were treated with a low insulin (50 pM) and low glucose (3.5 mM) plus 5 µM BODIPY-FFA (BODIPY FL C16) in the seven-channel microfluidic chip (only five channels used). The chip was placed and fixed on an inverted fluorescence microscope stage, equilibrated at 37 °C with humidity control. Vacuum was applied using a 60 mL syringe secured by tygon tubing attached to the microfluidic channels. After loading adipocyte explant, flow was started immediately. Real-time fluorescence was recorded in the parallel channels and saved in tagged image format (tif file) at 10 second intervals for 30 min.

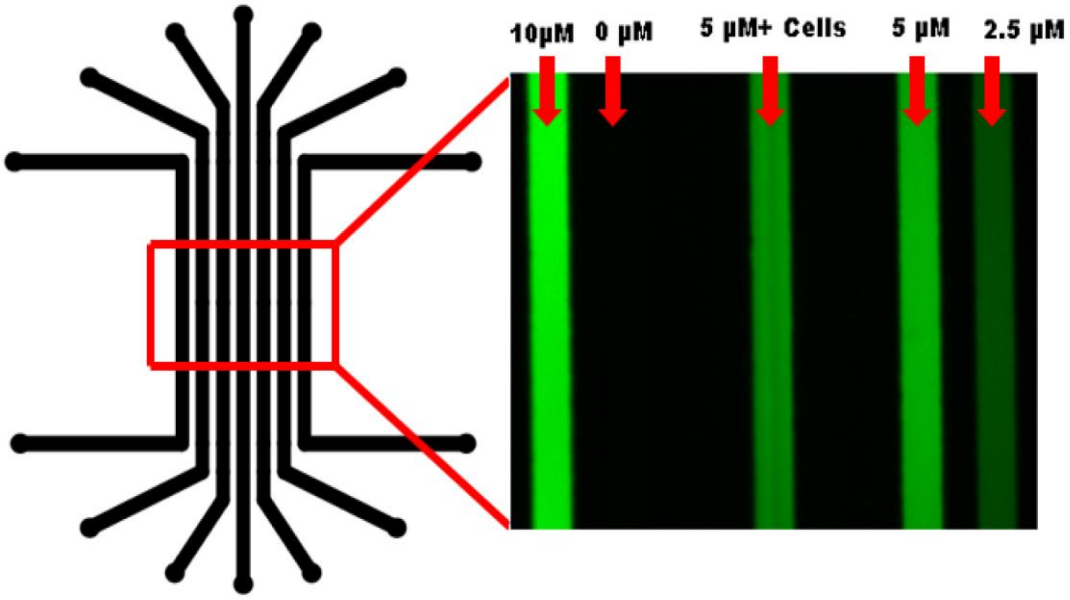

Fig.3.6 A seven-channel microfluidic chip layout (left) and representative fluorescence image controlled at the defined ROI

After 30 min, flow was stopped in every channel. The well with the adipose tissue explant was emptied and replaced with a high insulin (100 nM) and high glucose (11 mM) with 5 µM BODIPY-FFA (BODIPY FL C16). Vacuum was applied and flow controlled as before. Real-

time fluorescence images were recorded as above, and continuous calibration curves were used to determine the BODIPY-FFA concentrations in the channels. Images were analyzed using ImageJ, and finally uptake kinetics were calculated using Microsoft Excel.

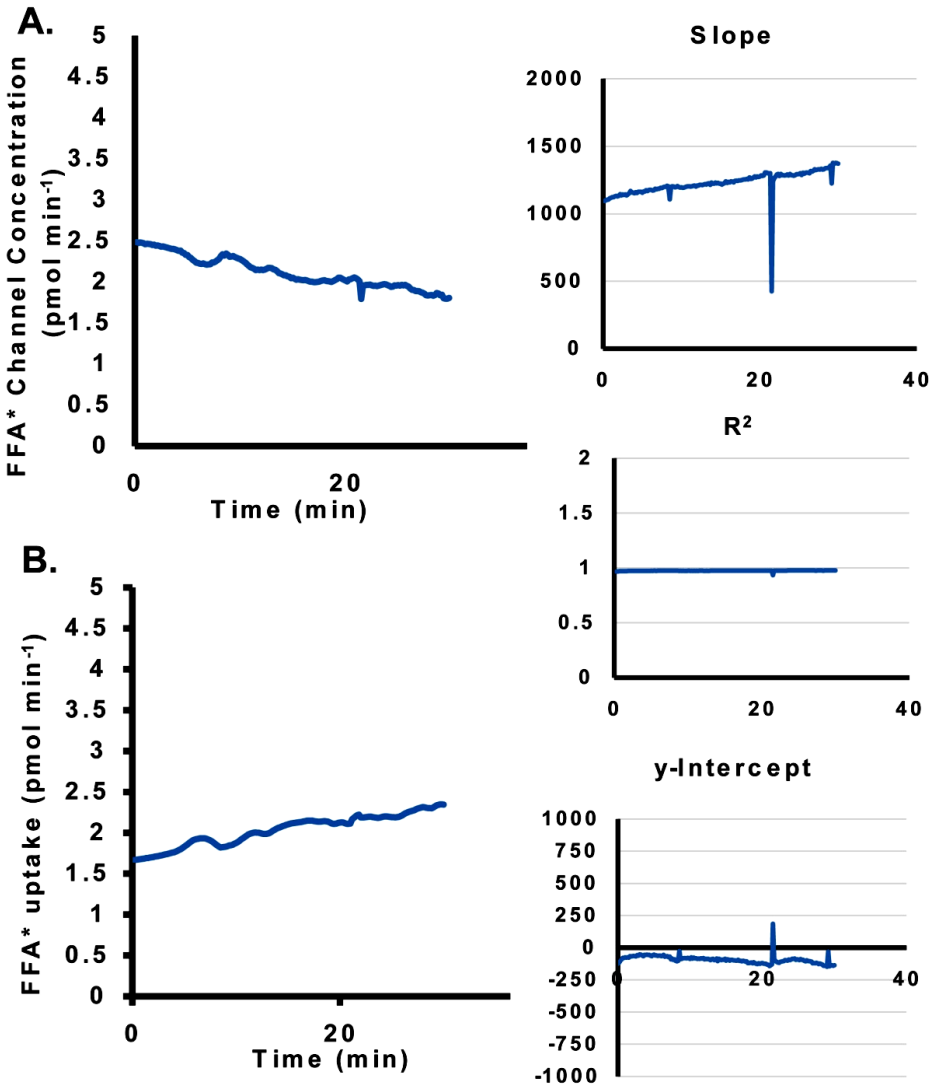

Fig.3.7 BODIPY FL C16 uptake kinetics: A) Decreasing concentration of the well with Explant when the same initial conc. of BODIPY-FFA (5µM) was given B) Shows increasing concentration in pmol min^{-1} going in to cells. The conc. Of BODIPY-FFA given initially was 5µM. On the right side is slope, R^2 and y-intercept of individual control channels throughout the meassurment time

We monitored the fluorescence of the solutions at the ROI defined in **Fig. 3.6**, and as the explants started taking-in the reagent we could later quantify the ammount absorbed by real-time

calibration with the standards in the other channels.This can be seen in **Fig.3.7B** where we observed increasing concentration (in Pmol/min) of our reagent going in to cells, along with some dynamic functions (not attributable to background). The uptake continued steadily from around 1.5 pmol/min, measured just after starting flow, to around 3 pmol/min towards the end of measurment time (30 minutes). Furthermore the channel with explant was analized and it can be seen that, its concentration continuously decreases after we start interogating the explant (**Fig. 3.7A**). From this finding we are convinced that our system works and that we were able to continuously flow our reagent over the explant and simultanously meassure how much of BODIPY-FFA is actually being taken. By including the calibration channels and analyzing them simultanously (**Fig.3.7** right side figures), this system allowed us not only to meassure the BODIPY-FFA uptake qualitatively but also able to quantify it in real-time with out any interference from optical drift. Another important advantage is that we can monitor BODIPY-FFA uptake without directly hitting cells with excitation light.

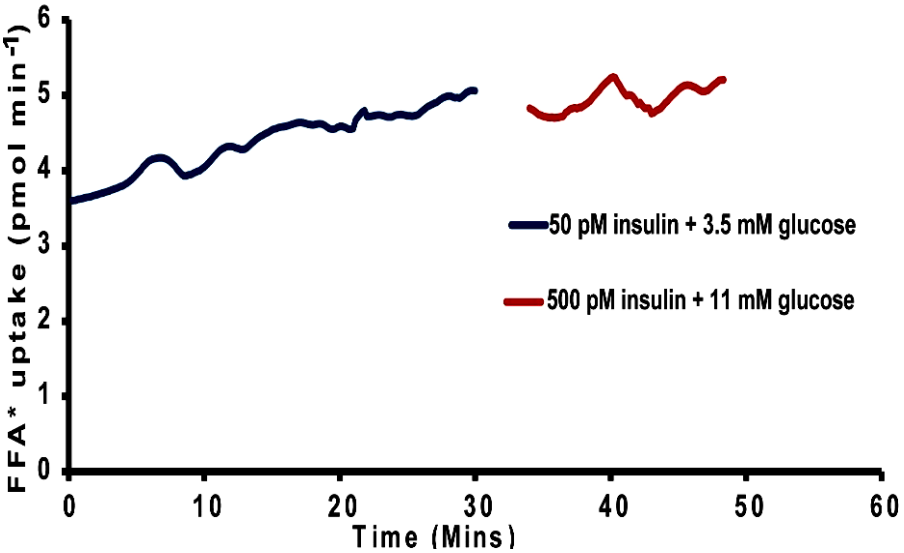

Fig.3.8 BODIPY FL C16 uptake kinetics after switching to High insulin/glucose (red trace)

As shown in **Fig. 3.8**, after 30 minutes, the solution in the well with explant and channel were emptied and replaced with 100 nM Insulin plus 11 mM glucose solution (High Insulin/Glucose). Flow was continued for the next 10 min. As shown in the figures, we did not observe significant differences in uptake kinetics with the high Insulin/Glucose treatment. Uptake remained practically the same. One reason could be that this time period was too short for explant to adjust and respond to the new solution.

The results shown here helped confirm that we could quantify BODIPY-FFA changes in the microchannels in real time using continuous calibration and that BODIPY-FFA uptake into cells could be determined. However, dynamic information was limited. These initial experiments exposed a weakness in our device design. Laminar flow allowed us to observe an undesirable effect due to our method of sampling from explants. In **Fig.3.6** above, we see differing intensity of fluorescence across the channel that sampled from the explant. It appears that this phenomenon was occurring because initially the channel would be flowing concentrated reagent, but after adding explant, the part of explant in the well closer to the channel was quickly taking up more reagent., but concentrated reagent was flowing around the explant nonetheless. This was problematic in our attempt to quantitatively assess the amount ofdyanmics of BODIPY-FFA taken up by the explant. As discussed below, we later solved this problem by introducing a foot-shaped region in our macro-to-micro interface portion of the chip (see **Fig.3.11A&B**). This foot shaped region, made with a 3D-printed template (**Fig. 3.11C**), helped to hold explants immersed in solution, hence our reagent flow would be forced to interact with the explant rather than bypassing it.

3.3.5 Inhibition of BODIPY C16 uptake by Deoxycholic acid

Mainly found in the bile of mammals, bile acids are steroid acids synthesized in the liver by a process requiring more than a dozen enzymes. Primary bile acids are specifically synthesized in the liver from cholesterol and conjugated with taurine or glycine in the liver forming bile salts. They are normal components of the lumenal contents of the gastrointestinal (GI) tract, where they enable absorption of lipids, cholesterol, and fat-soluble vitamins by acting as physiologic detergents and they regulate intestinal epithelial homeostasis in the GI tract. Secondary bile acids are the result of bacterial actions in the colon[66,67].

Deoxycholic acid (DCA), a secondary bile acid has been widely used in medicine, as digestive aid in the food industry [68] and for reducing moderate-to-severe fat below the chin [69]. Although its mechanism is illusive there is published data that shows DCA inhibit uptake of BODIPY-FFA in adipocytes both in vitro and in vivo [70]. We have thus applied DCA to examine uptake inhibition in our system.

A 2-mm diameter adipocyte explant was incubated with 5 mM DCA in 5%CO_2 for 30 minutes. After washing with PBS, the explant was immediately transferred to the microfluidic chip on a microscope stage equilibrated to 37 $^{\circ}$C. A 5 µM BODIPY-FFA (BODIPY C16) with high insulin/glucose (100 nM/11 mM) was applied to the cells. Flow was started and fluorescence was measured in the channels with the same parameters as mentioned in **section 3.3.4**.

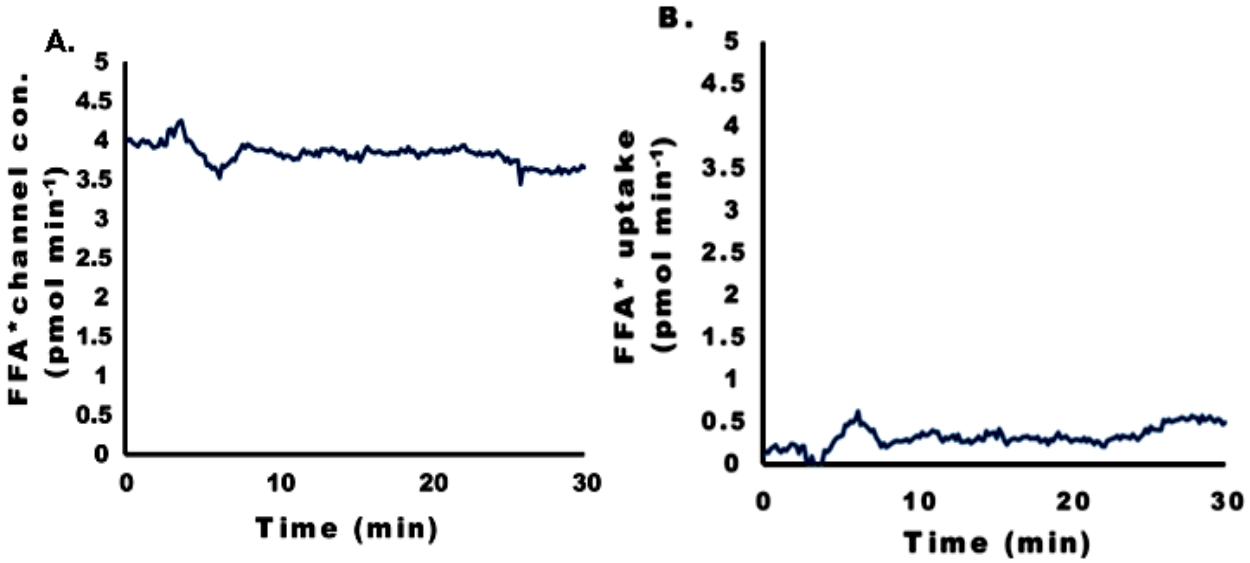

Fig.3.9 BODIPY C16 uptake under the effect of 5 mM Deoxycholic Acid (DCA) A) Concentration of channel with explant B) BODIPY-FFA (µM) taken by 2mm Dia. Explant

From **Fig. 3.9A** , we can see that the concentration in the channel with explant change only slightly for the entire duration of the experiment, which shows inhibition of the uptake by DCA. The actual BODIPY-FFA taken by the explant is shown by **Fig.3.9B**, which barely reaches 0.5 µM toward the end of the experiment . Although it is unclear if dynamic information was relevant with the first-generation device, these inhibition results at least confirmed that the device was quantitatively assessing the BODIPY-FFA uptake capabilities of adipose explants.

3.3.6 Second-generation microfluidic device for FFA uptake quantification

To correct several deficiencies in design and operation, several changes were made to give our second-generation device (**Fig. 3.10**). First, the number of sampling channels was reduced to 5, giving 3 for calibration and 2 for duplicate biological experiments (2 explants). The smaller number of channels ensured that spacing between channels was larger to prevent leakage and

ease device fabrication. The chip design and a typical image during sampling are shown in **Fig. 3.10.**

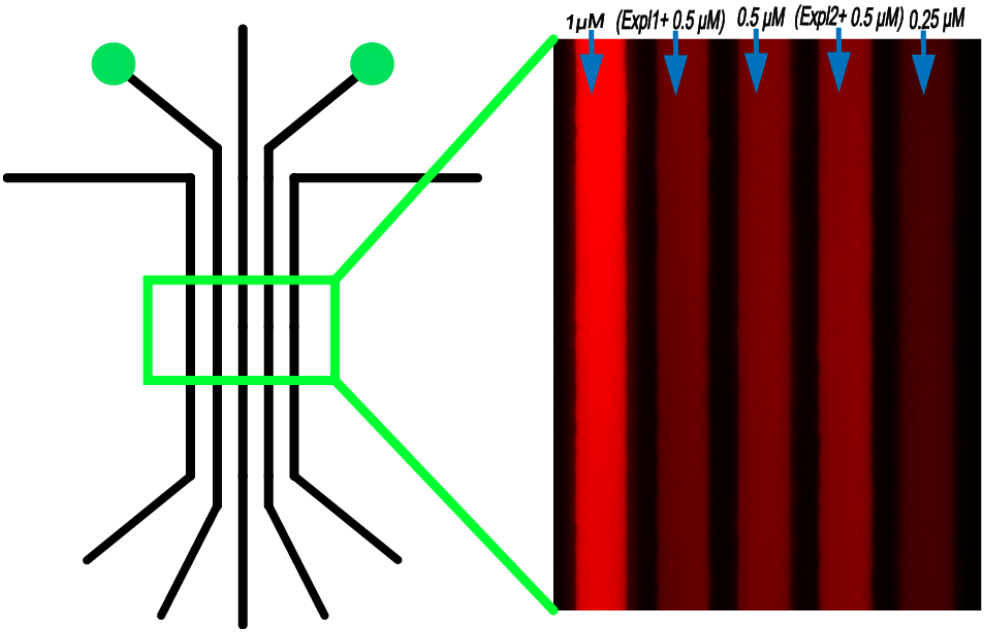

Fig.3.10 Fluorescence measurement area on second-generation microfluidic chip: The chip is designed in such a way that our reagent (BODIPY-FFA) will flow over the explant (green zone) after interrogating it. Downstream all the channels are in parallel (green rectangle). Fluorescence was measured continuously at this area and recorded as tagged image file (tif) for analysis.

Secondly, the cell interfacing method was improved. To ensure that the explant was stimulated and sampled continuously, a foot-shaped cell trapping region was included in our macro-to-micro interface portion of the chip (**Fig.3.11**). Building upon recent work from our group[40,39], this foot shaped region was made with a 3D-printed template (**Fig.3.11C**). This region helped to hold explants immersed in solution, and our reagent flow was forced to interact with the explant rather than bypassing it. An image of the completed device with two explant sampling regions is shown in **Fig. 3.11A**, and a cross-section of the macro-to-micro interface is shown in **Fig. 3.11B**.

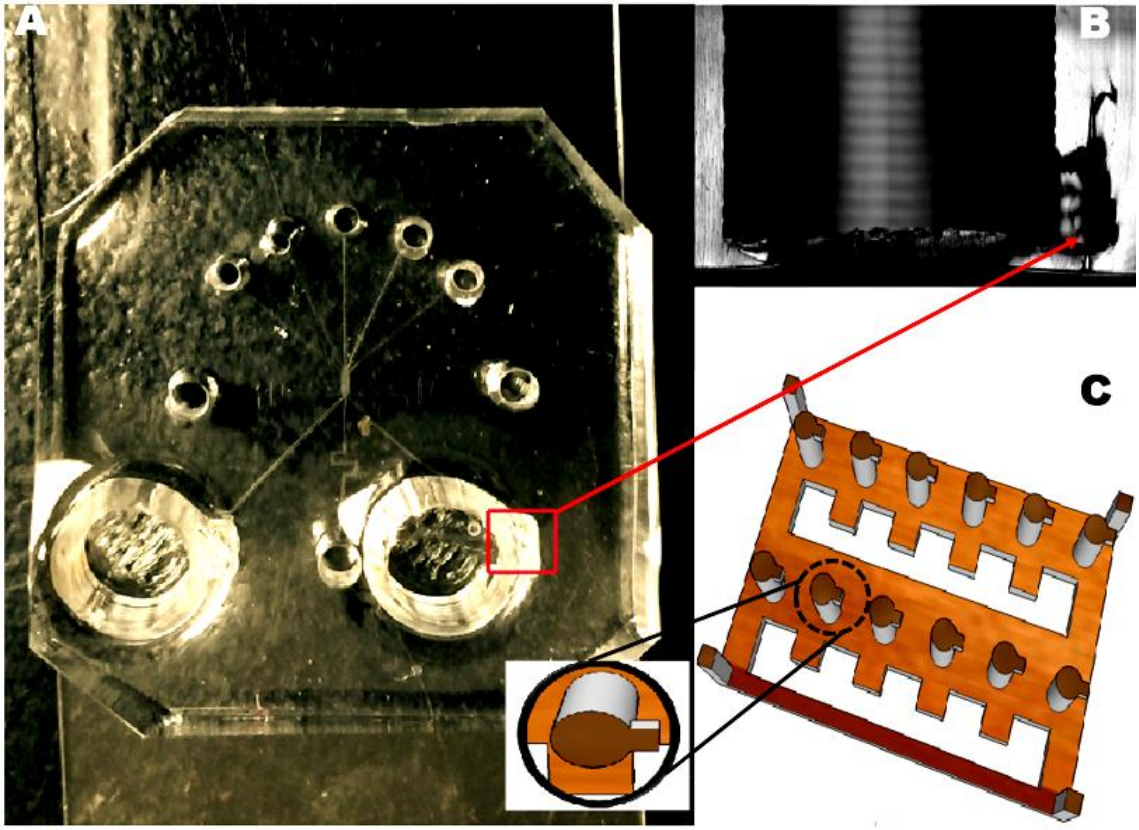

Fig. 3.11 Five channel chip and explant Trap made with 3D-printed template: A) a five channel chip with two wells for explant interrogation and a foot-shaped trap (shown by red rectangle) to prevent the explant from floating. B) Shown by the red arrow is a zoomed-in cross sectional view of the foot and a via made with CO2 laser. The via allows the solution to flow freely over the explants to the channel downstream were fluorescence is measured. C) 3D-printed template used to make the foot-shaped well-trap for explants

The second-generation device was used to analyze BODIPY-FFA (BODIPY C12) uptake by explants. Two 3-mm Explants were interrogated under, 100 nM insulin with 20 mM glucose (High) and two other 3-mm explants were interrogated under, 50 pM insulin with 5.5 mM glucose (Low) in two separate experiments. To account for free fatty acids floating around in plasma as a result of lipolysis and De novo synthesis, explants were pre-incubated with 0.5 µM unlabeled lauric acid (C12) for one hour. Explants were washed with warm PBS and transferred to BSA-treated microfluidic chip equilibrated to 37 °C on a microscope stage. Flow was started by applying vacuum from a hand-held 100 mL syringe attached to a homemade manifold

(**Fig.3.3**). **Fig.3.12** shows the real-time uptake kinetics observed under the high (**Fig.3.12A**) and low (**Fig.3.12B**) insulin/glucose treatments. As before, calibration channels were analyzed simultaneously and were used to quantify uptake. A combined view of the uptake kinetics of the four different explants is given in **Fig. 3.13**. Represented by the insert in **fig.3.13** is the total amount of the BODIPY-FFA being stored over time. These explants were taken from the same mouse but should represent slightly different locations of the same fat pad.

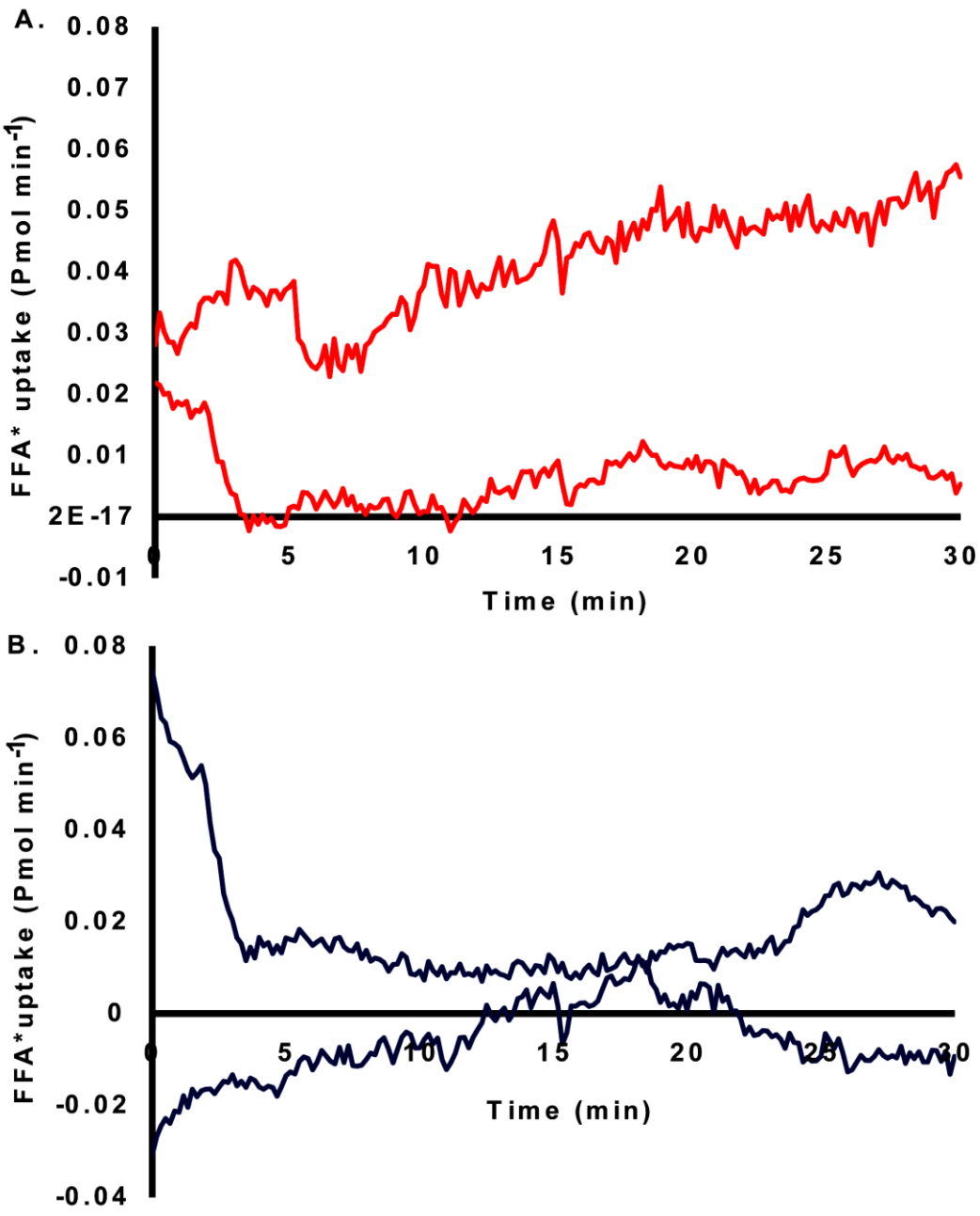

Fig.3.12 Individual BODIPY-FFA uptake traces A) 0.5 µM BODIPY-FFA plus 100 nM insulin and 20 mM glucose (High) B) 0.5 µM BODIPY-FFA plus 50 pM insulin and 5.5 mM glucose (Low)

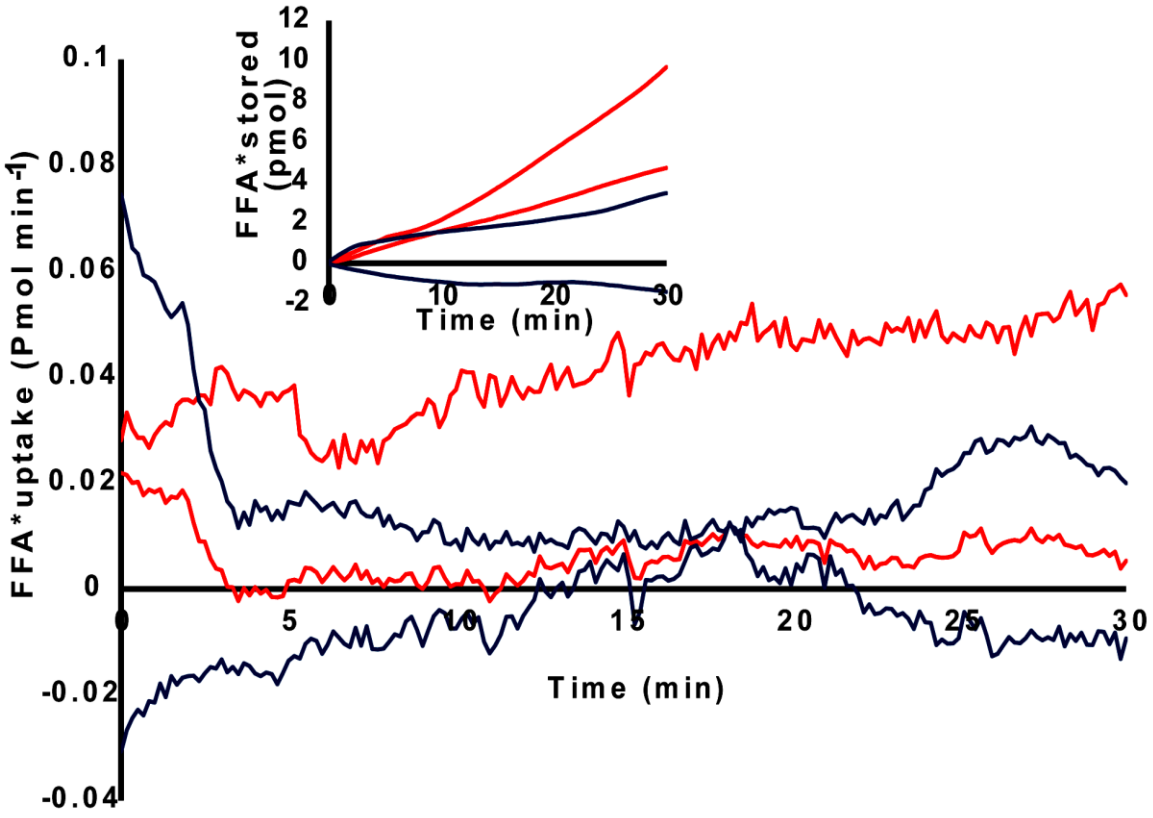

Fig.3.13 Combined uptake kinetics from four explants; Red traces represent uptake kinetics(pmol/min) of two explants treated with 100 nM Insulin plus 20 mM glucose, Blue traces represent uptake kinetics (pmol/min) of two explants treated with 50 pM Insulin plus 5.5 mM glucose. Insert represents BODIPY-FFA stored in the explants (in pmols) over the 30 min assay time.

3.4 Co-uptake of fatty acids and a glucose analogue by Adipose tissue explants using our microfluidic system

2-NBDG (2-(N-(7-Nitrobenz-2-oxa-1, 3-diazol-4-yl) Amino)-2-Deoxyglucose) is a fluorescent glucose analog that has been used to monitor glucose uptake in live cells and as an indicator of cell viability. First synthesized by Yoshioka K. in 1996[71],This reagent with typical excitation/emission maxima at ~465/540 nm, has been widely used to determine direct glucose uptake in diabetic studies[72], real-time imaging of glucose in single mammalian cells[73] and many other applications involving glucose.

Here we used our second-generation device to simultaneously measure the uptake kinetics of 2-NBDG and BODIPY C12 by adipocyte tissue explants.

The "glucose-fatty acid cycle" otherwise called the Randle cycle, proposed by Randle in 1963, explains the biochemical mechanism involving competition between glucose and fatty acids for their oxidation and uptake in muscle and adipose tissue. The cycle controls fuel selection and adapts the substrate supply and demand in normal tissues. According to Randle this cycle involves two features, restrictions imposed on glucose metabolism in muscle by the release of more fatty acids for oxidation (derived from muscle or adipose-tissue TAGs), and those restrictions imposed on release of fatty acids from TAGs by uptake of glucose[74]. We now know that in the fasting state, activation of lipolysis provides tissues with fatty acids as preferred fuel for respiration and β-oxidation of fatty acids produces ketone bodies which are preferentially oxidized in extrahepatic tissues. By inhibiting glucose oxidation, fatty acids and ketone bodies contribute to a glucose-sparing effect, which in turn preserves glucose for tissues like the brain. In non-fasting state (fed state), say after a high-fat meal or during exercise, when plasma concentrations of fatty acids or ketone bodies increase, part of the glucose that is not oxidized is redirected to glycogen. Rapid synthesis of glycogen in muscle after exercise and increased glycogen content in muscles found in starvation or diabetes are the result of this processes. The mechanism by which glucose uptake inhibits fatty acid oxidation is mediated by glucose-derived malonyl-CoA, which inhibits the entry of long-chain fatty acyl (LCFAcyl-CoA) moieties into mitochondria. This effect redirects fatty acids toward esterification. This process also controls lipogenesis in the long term favoring carbohydrate storage into lipid rather than oxidation of glucose itself[75,76,77].

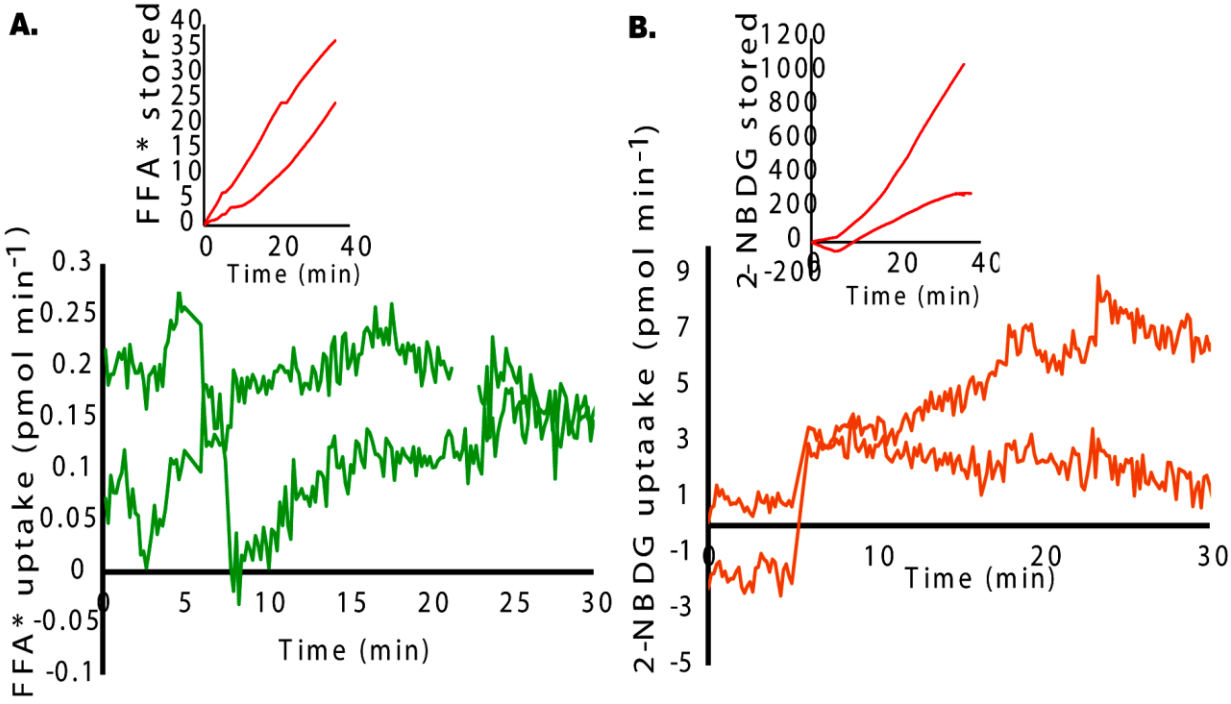

Fig.3.14 Uptake kinetics of two explants A) BODIPY C12 and B) 2-NBDG channels analyzed separately; the insert represents the amount of each substrate (pmol) stored over time

In this experiment, we aimed at applying our chip in studying the co-uptake of glucose and fatty acid. For this experiment, two 2-mm diameter (wet volume) adipose tissue explants were incubated with 3 µM BODIPY labeled FFA C12, 50 µM 2-NBDG plus 50 pM insulin and 5.5 mM glucose (Low insulin/glucose) for one hour at 37 $^{\circ}$C and 5%CO_2. After this cells were washed with PBS, and transferred to the chip on the microscope stage equilibrated at 37 $^{\circ}$C. We made sure that the explant was trapped in the foot region of the chip made with the 3D-printed template. Cells were treated with 3 µM BODIPY C12, 50 µM 2-NBDG plus 100 nM Insulin and 5.5 mM Glucose (High Insulin/Low Glucose) during sampling and imaging. Finally, flow was started and measurement was done at 10 s intervals for 30 min.

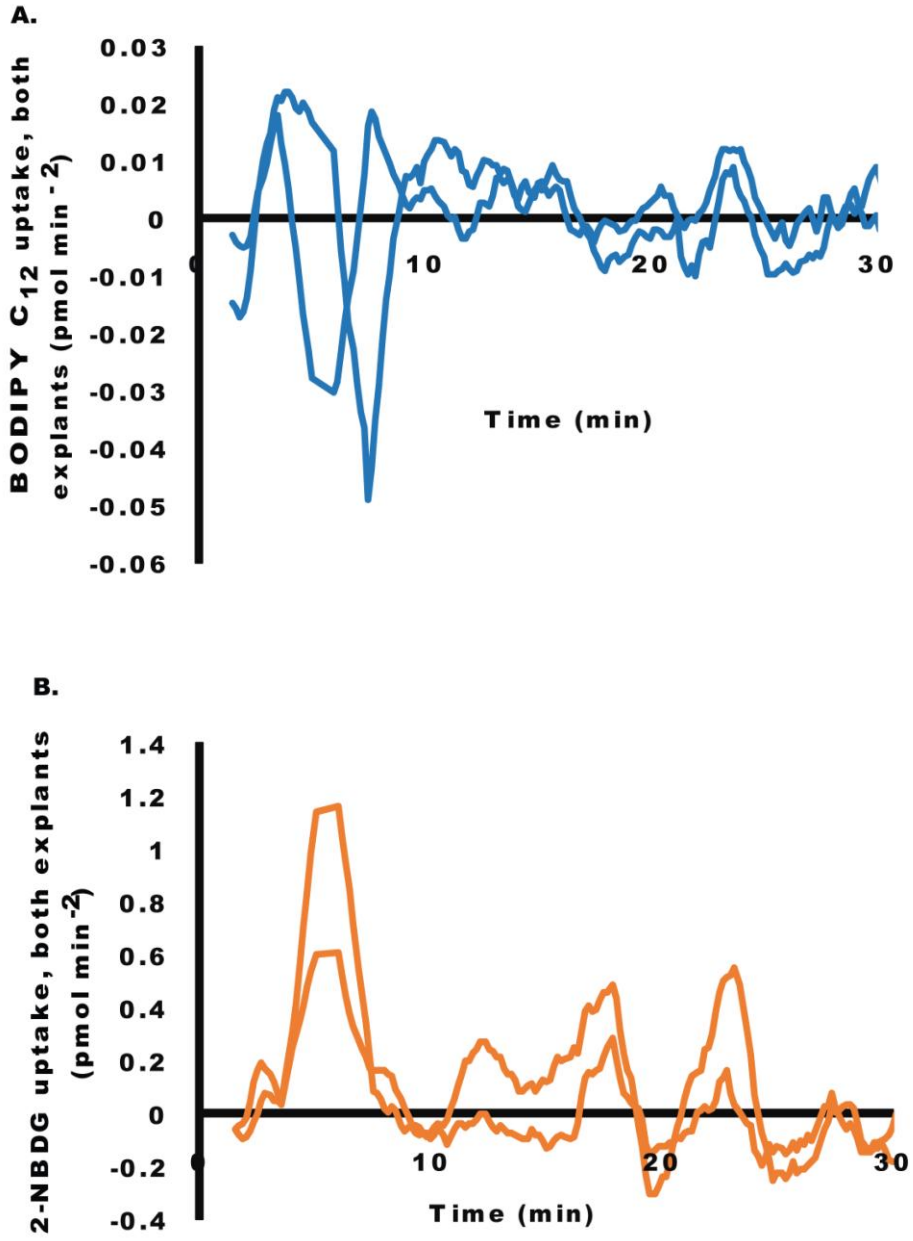

Fig.3.15 Derivative of the uptake kinetics of two explants A) BODIPY C12 and B) 2-NBDG computed for comparison of the trend of the co-uptake

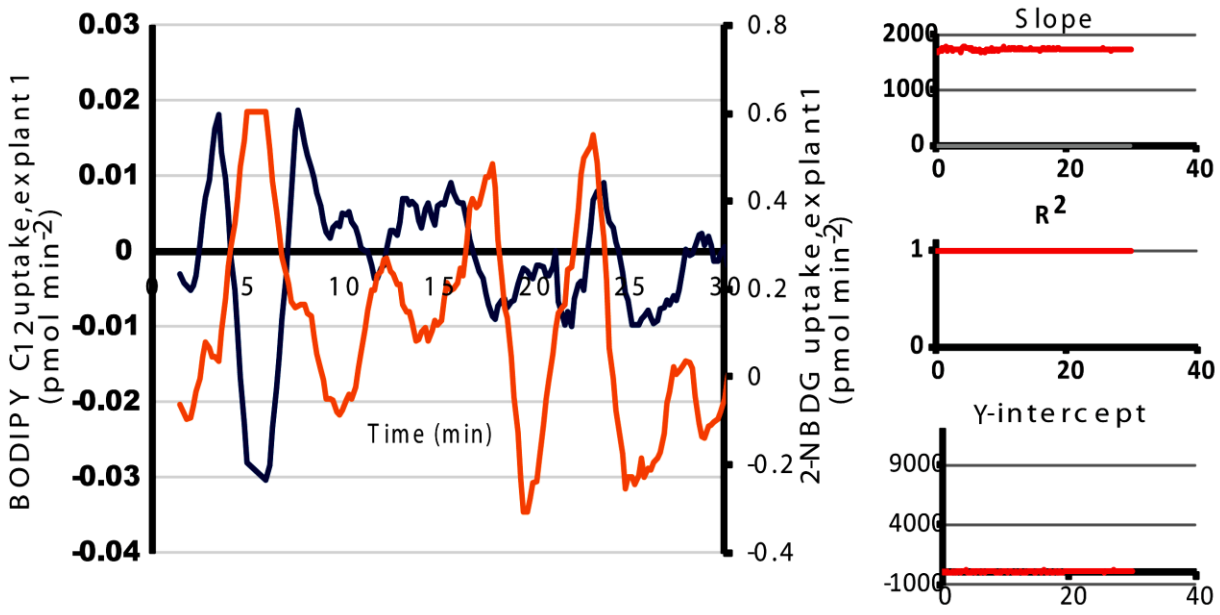

Fig. 3.16 A) Combined uptake derivative of Bodipy C12 (blue trace) and 2-NBDG (orange trace) for explant1; B) Slope, R^2 and y-intercept of calibration channels

The results in **Fig.3.14A** and **B** show the uptake of these two substrates. Although this data is preliminary, from the derivative uptake data shown by **Fig.15 A** and **B**, it appears that 2-NBDG and BODIPY-FFA uptake rates were opposing each other in time for much of the experiment. In other words, uptake of BODIPY-FFA was accompanied by release of 2-NBDG, and vice versa. **Fig.3.16A** which represents the combined uptake derivative (BODIPY C12 and 2-NBDG) for one of the explants (explant1) clearly demonstrates the aforementioned claim. This would be consistent with FFA uptake inhibiting glucose utilization, although the reasons behind the dynamic fluctuations are unclear. These results help to illustrate how microfluidics can provide novel information on biological systems, and these patterns shown by adipose tissue should be explored further in future studies.

CHAPTER 4

Conclusion and Future Directions

4.1 Conclusions

The ability of white adipose tissue to efficiently take up fatty acids (long-chain fatty acids) is a key to its physiological function in energy storage. The major purpose of this study was to develop a real-time and quantitative fatty acid uptake assay for adipose tissue (white adipose tissue) that circumvents the key drawbacks in the previously reported techniques. By far the most challenging issues in those techniques has been avoiding direct excitation light during imaging which would otherwise damage the cells and create complication of end results due to photo bleaching. In our approach in this study we applied a unique design of the commercial microplate made in our lab. We custom made it to include a small moat area which confine cells and gave as the ability to focus the excitation light to a small, cell free region in the solution. While cells take up the fluorescently labelled fatty acid, change in fluorescence was measured without exposing cells to direct exciting light. We had minor issue with the printed microplate, which we know could easily be solved with a better printing material. Another major weakness in the previously reported assay techniques is lack of good mimic of the physiological environment because almost all of the available uptake assays depend on designing an uptake assay around end point fluorescence measurement and mostly for attached 3T3-L1 adipocytes. These approaches overlook two main facts, one the 3T3-L1 cells are not a good representation of real adipose tissue and hence the results cannot be extrapolated with confidence. The previous techniques also use radioactive fatty acids and several expensive instruments with protocols that need extra skill such as microinjecting cells with fatty acids. In our second project in this study, we have used microfluidics to design a flowing system and used adipose tissue explants which,

in combination resulted in an assay system with excellent mimic of physiological environment. Furthermore for all our study we employed commercially available fluorescently labelled fatty acids (BODIPY-labelled FFAs) which are cheap, nontoxic and very similar in uptake behavior to natural fatty acids. From the results we obtained, with minor issues in flow rate control for longer assay times, we achieved our goal of designing a real-time, quantitative assay for the uptake of free fatty acid in adipose tissue. We believe that our assay system developed in this study can be improved further as described below.

4.2 Future uptake analysis in flowing systems applying active valving

The Quake group led the way to the fabrication and application of microfluidic systems containing on-off valves, switching valves, and pumps exclusively made of the substrate elastomer material, PDMS. The technique they called "multilayer soft lithography" combines soft lithography with the capability to bond multiple patterned layers of elastomer. Multilayer structures (**Fig. 4.1A**) are constructed by bonding layers of elastomer, each of which is separately cast from a micro-patterned mold. These valves work on a simple principle, which is pressure-driven deformation of PDMS from one channel (below or above) blocking the flow in the intersecting channels from the other layers[78],[79].

PDMS valves have the merits of relatively simple fabrication, high compliance, low cost, and good biocompatibility. These valves are popular in use mainly because they can be easily integrated with standard soft lithography processes.

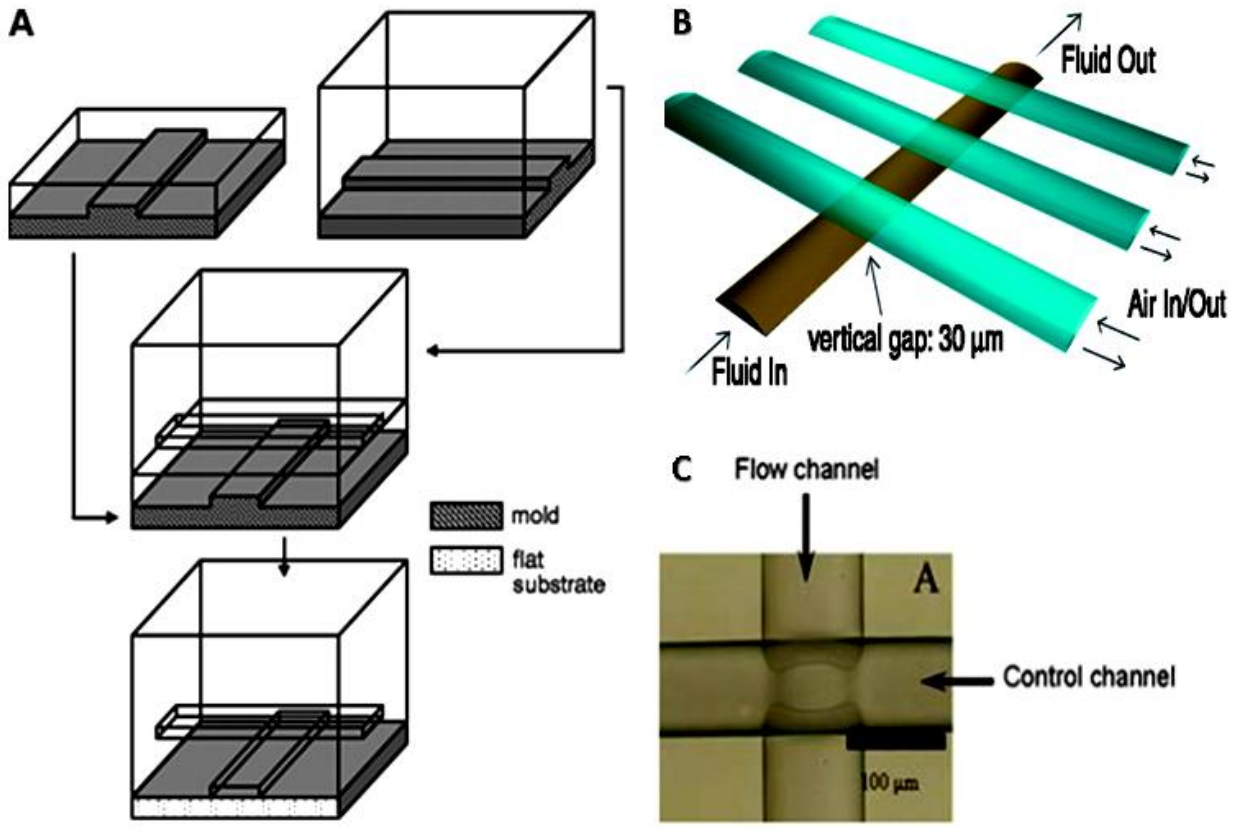

Fig.4.1 A) Process flow for multilayer soft lithography B) A 3D scale diagram of an elastomeric peristaltic pump and C) Microscopy image of an activated Quake valve

In the systems presented in this thesis, the main challenges we encountered using our flowing systems was maintaining a steady flow rate for long periods of time. The passively operated flow rate control applying manifold works very well, yet with constant variation of the temperature and pressure of the environment (lab) it is difficult to maintain a stable and continuous flow rate for extended time while cells are being interrogated. Both in our lab[39,49]and others, the application of pneumatic valves made with elastomer has helped automate microfluidic flow rate. We believe the same principle can greatly improve the accuracy of the real-time free fatty acid uptake in our device. For example, in a hypothetical third-generation device, valve-based peristaltic pumps could be used to apply a sustained flow rate for hours, and the system would be fully automated for continuous calibration and sampling. With these improvements, dynamic

changes such as those shown in **Fig. 3.13** could be further investigated with higher chip-to-chip consistency. On-chip peristaltic pumps as in **Fig. 4.1B** also provide excellent control over flow rates, which would further improve our precision of quantifying the amounts of BODIPY-FFA taken up by cells over time.

References:

(1) Liao, J.; Sportsman, R.; Harris, J.; Stahl, A. *J. Lipid Res.* **2005**, *46* (3), 597–602.

(2) Macdougald, O. A. *Methods in enzymology. Volume five hundred and thirty eight, Volume five hundred and thirty eight,*; 2014.

(3) Kampf, J. P.; Kleinfeld, A. M. *J. Biol. Chem.* **2004**, *279* (34), 35775–35780.

(4) Simard, J.; Kamp, F.; Hamilton, J. In *Methods in Membrane Lipids*; Dopico, A., Ed.; Methods in Molecular Biology™; Humana Press, **2007**; pp 27–43.

(5) Kasurinen, J. *Biochem. Biophys. Res. Commun.* **1992**, *187* (3), 1594–1601.

(6) WHO | Diabetes http://www.who.int/mediacentre/factsheets/fs312/en/ (accessed Feb 28, 2016).

(7) Park, A.; Kim, W. K.; Bae, K.-H. *World J. Stem Cells* **2014**, *6* (1), 33–42.

(8) Lee, M.-J.; Wu, Y.; Fried, S. K. *Mol. Aspects Med.* **2013**, *34* (1), 1–11.

(9) Kajimura, S.; Seale, P.; Spiegelman, B. M. *Cell Metab.* **2010**, *11* (4), 257–262.

(10) *IUPAC Compendium of Chemical Terminology: Gold Book*, 2.1.0.; Nič, M., Jirát, J., Košata, B., Jenkins, A., McNaught, A., Eds.; IUPAC: Research Triagle Park, NC, 2009.

(11) Offermanns, S. *Annu. Rev. Pharmacol. Toxicol.* **2014**, *54*, 407–434.

(12) Fatty Acid Synthesis http://www.rpi.edu/dept/bcbp/molbiochem/MBWeb/mb2/part1/fasynthesis.htm (accessed Mar 2, 2017).

(13) Kershaw, E. E.; Flier, J. S. *J. Clin. Endocrinol. Metab.* **2004**, *89* (6), 2548–2556.

(14) Boden, G. *Endocrinol. Metab. Clin. North Am.* **2008**, *37* (3), 635–646, viii–ix.

(15) Reaven, G. M.; Hollenbeck, C.; Jeng, C. Y.; Wu, M. S.; Chen, Y. D. *Diabetes* **1988**, *37* (8), 1020–1024.

(16) Boden, G.; Chen, X.; Ruiz, J.; White, J. V.; Rossetti, L. *J. Clin. Invest.* **1994**, *93* (6), 2438–2446.

(17) Santomauro, A. T.; Boden, G.; Silva, M. E.; Rocha, D. M.; Santos, R. F.; Ursich, M. J.; Strassmann, P. G.; Wajchenberg, B. L. *Diabetes* **1999**, *48* (9), 1836–1841.

(18) Treibs, A.; Kreuzer, F.-H. *Justus Liebigs Ann. Chem.* **1968**, *718* (1), 208–223.

(19) BODIPY Dye Series—Section 1.4 https://www.thermofisher.com/us/en/home/references/molecular-probes-the-handbook/fluorophores-and-their-amine-reactive-derivatives/bodipy-dye-series.html (accessed Dec 15, 2016).

(20) Kowada, T.; Maeda, H.; Kikuchi, K. *Chem. Soc. Rev.* **2015**, *44* (14), 4953–4972.

(21) Stahl, A.; Evans, J. G.; Pattel, S.; Hirsch, D.; Lodish, H. F. *Dev. Cell* **2002**, *2* (4), 477–488.

(22) Li, H.; Black, P. N.; DiRusso, C. C. *Anal. Biochem.* **2005**, *336* (1), 11–19.

(23) Varlamov, O.; Somwar, R.; Cornea, A.; Kievit, P.; Grove, K. L.; Roberts, C. T. *Am. J. Physiol. - Endocrinol. Metab.* **2010**, *299* (3), E486–E496.

(24) Somwar, R.; Roberts, C. T.; Varlamov, O. *FEBS Lett.* **2011**, *585* (12), 1946–1950.

(25) Chu, M.; Sampath, H.; Cahana, D. Y.; Kahl, C. A.; Somwar, R.; Cornea, A.; Roberts, C. T.; Varlamov, O. *Mol. Biol. Cell* **2014**, *25* (25), 4096–4105.

(26) Varlamov, O.; Chu, M.; Cornea, A.; Sampath, H.; Roberts, C. T. *Endocrinology* **2015**, *156* (1), 80–89.

(27) Kazantzis, M.; Stahl, A. *Biochim. Biophys. Acta* **2012**, *1821* (5), 852–857.

(28) Cm, A.; A, S. *Mol. Asp. Med. Mol. Asp. Med.* **2013**, *34*, *34* (2–3, 2–3), 516, 516–528.

(29) Abumrad, N.; Coburn, C.; Ibrahimi, A. *Biochim. Biophys. Acta* **1999**, *1441* (1), 4–13.

(30) Gossett, R. E.; Frolov, A. A.; Roths, J. B.; Behnke, W. D.; Kier, A. B.; Schroeder, F. *Lipids* **1996**, *31* (9), 895–918.

(31) Storch, J.; Thumser, A. E. *Biochim. Biophys. Acta* **2000**, *1486* (1), 28–44.

(32) Bernlohr, D. A.; Coe, N. R.; LiCata, V. J. *Semin. Cell Dev. Biol.* **1999**, *10* (1), 43–49.

(33) Doege, H.; Stahl, A. *Physiology* **2006**, *21* (4), 259–268.

(34) Stahl, A. *Pflüg. Arch. Eur. J. Physiol.* **2004**, *447* (5), 722–727.

(35) Su, X.; Abumrad, N. A. *Trends Endocrinol. Metab. TEM* **2009**, *20* (2), 72–77.

(36) Hui, T. Y.; Bernlohr, D. A. *Front. Biosci. J. Virtual Libr.* **1997**, *2*, d222-231.

(37) Berk, P. D.; Stump, D. *Hepatol. Baltim. Md* **1999**, *29* (5), 1607–1609.

(38) Fedorenko, A.; Lishko, P. V.; Kirichok, Y. *Cell* **2012**, *151* (2), 400–413.

(39) Li, X.; Brooks, J. C.; Hu, J.; Ford, K. I.; Easley, C. J. *Lab. Chip* **2017**, *17* (2), 341–349.

(40) Brooks, J. C.; Ford, K. I.; Holder, D. H.; Holtan, M. D.; Easley, C. J. *Analyst* **2016**, *141* (20), 5714–5721.

(41) Cypess, A. M.; Kahn, C. R. *Curr. Opin. Pediatr.* **2010**, *22* (4), 478–484.

(42) Henkin, A. H.; Cohen, A. S.; Dubikovskaya, E. A.; Park, H. M.; Nikitin, G. F.; Auzias, M. G.; Kazantzis, M.; Bertozzi, C. R.; Stahl, A. *ACS Chem. Biol.* **2012**, *7* (11), 1884–1891.

(43) Godinat, A.; Budin, G.; Molares, A. R.; Park, H. M.; Sanman, L. E.; Bogyo, M.; Yu, A.; Stahl, A.; Dubikovskaya, E. A. *Curr. Protoc. Chem. Biol.* **2014**, *6* (3), 169–189.

(44) Photobleaching - MeSH - NCBI https://www.ncbi.nlm.nih.gov/mesh/68038761 (accessed Feb 14, 2017).

(45) Hoebe, R. A.; Van Oven, C. H.; Gadella, T. W. J.; Dhonukshe, P. B.; Van Noorden, C. J. F.; Manders, E. M. M. *Nat. Biotechnol.* **2007**, *25* (2), 249–253.

(46) Ji, N.; Shroff, H.; Zhong, H.; Betzig, E. *Curr. Opin. Neurobiol.* **2008**, *18* (6), 605–616.

(47) He, Y.; Wu, Y.; Fu, J.; Gao, Q.; Qiu, J. *Electroanalysis* **2016**, *28* (8), 1658–1678.

(48) Jeremy Rifkin and the Third Industrial Revolution http://www.thethirdindustrialrevolution.com/ (accessed Feb 14, 2017).

(49) Jean T. Negou, L. Adriana Avila, Tesfagebriel M. Hagos, and Christopher J. Easley. Anal. Chem. 2017. (***Submitted***)

(50) Pohl, J.; Ring, A.; Korkmaz, Ü.; Ehehalt, R.; Stremmel, W. *Mol. Biol. Cell* **2005**, *16* (1), 24–31.

(51) Godwin, L. A.; Brooks, J. C.; Hoepfner, L. D.; Wanders, D.; Judd, R. L.; Easley, C. J. *The Analyst* **2015**, *140* (4), 1019–1025.

(52) Smitka, K.; Marešová, D. *Prague Med. Rep.* **2015**, *116* (2), 87.

(53) Frühbeck, G.; Salvador, J. *Nutr. Res.* **2004**, *24* (10), 803–826.

(54) Booth, A.; Magnuson, A.; Fouts, J.; Foster, M. T. *Horm. Mol. Biol. Clin. Investig.* **2016**.

(55) Romere, C.; Duerrschmid, C.; Bournat, J.; Constable, P.; Jain, M.; Xia, F.; Saha, P. K.; Del Solar, M.; Zhu, B.; York, B.; Sarkar, P.; Rendon, D. A.; Gaber, M. W.; LeMaire, S. A.; Coselli, J. S.; Milewicz, D. M.; Sutton, V. R.; Butte, N. F.; Moore, D. D.; Chopra, A. R. *Cell* **2016**, *165* (3), 566–579.

(56) Funaki, M. *J. Med. Investig. JMI* **2009**, *56* (3–4), 88–92.

(57) Mampallil, D.; George, S. D. *Resonance* **2012**, *17* (7), 682–690.

(58) Squires, T. M.; Quake, S. R. *Rev. Mod. Phys.* **2005**, *77* (3), 977–1026.

(59) Dugan, C. E.; Kennedy, R. T. *Methods Enzymol.* **2014**, *538*, 195–209.

(60) Roper, M. G.; Shackman, J. G.; Dahlgren, G. M.; Kennedy, R. T. *Anal. Chem.* **2003**, *75* (18), 4711–4717.

(61) Adewola, A. F.; Lee, D.; Harvat, T.; Mohammed, J.; Eddington, D. T.; Oberholzer, J.; Wang, Y. *Biomed. Microdevices* **2010**, *12* (3), 409–417.

(62) Shaikh Mohammed, J.; Wang, Y.; Harvat, T. A.; Oberholzer, J.; Eddington, D. T. *Lab. Chip* **2009**, *9* (1), 97–106.

(63) Volpatti, L. R.; Yetisen, A. K. *Trends Biotechnol.* **2014**, *32* (7), 347–350.

(64) Brooks, J. C.; Judd, R. L.; Easley, C. J. *Methods Mol. Biol. Clifton NJ* **2017**, *1566*, 185–201.

(65) Geng, T.; Zhan, Y.; Wang, J.; Lu, C. *Nat. Protoc.* **2011**, *6* (8), 1192–1208.

(66) Russell, D. W. The Enzymes, Regulation, and Genetics of Bile Acid Synthesis http://www.annualreviews.org/doi/10.1146/annurev.biochem.72.121801.161712 (Accessed Feb 3, 2017).

(67) Ajouz, H.; Mukherji, D.; Shamseddine, A. *World J. Surg. Oncol.* **2014**, *12*, 164.

(68) Deoxycholic Acid *https://en.wikipedia.org/wiki/Deoxycholic_acid*. (Accessed, March 26, 2017)

(69) Press Announcements - FDA approves treatment for fat below the chin http://www.fda.gov/NewsEvents/Newsroom/PressAnnouncements/ucm444978.htm (accessed Feb 3, 2017).

(70) Nie, B.; Park, H. M.; Kazantzis, M.; Lin, M.; Henkin, A.; Ng, S.; Song, S.; Chen, Y.; Tran, H.; Lai, R.; Her, C.; Maher, J. J.; Forman, B. M.; Stahl, A. *Hepatol. Baltim. Md* **2012**, *56* (4), 1300–1310.

(71) Yoshioka, K.; Takahashi, H.; Homma, T.; Saito, M.; Oh, K. B.; Nemoto, Y.; Matsuoka, H. *Biochim. Biophys. Acta* **1996**, *1289* (1), 5–9.

(72) Zou, C.; Wang, Y.; Shen, Z. *J. Biochem. Biophys. Methods* **2005**, *64* (3), 207–215.

(73) Yamada, K.; Saito, M.; Matsuoka, H.; Inagaki, N. *Nat. Protoc.* **2007**, *2* (3), 753–762.

(74) Randle, P. J.; Garland, P. B.; Hales, C. N.; Newsholme, E. A. *Lancet Lond. Engl.* **1963**, *1* (7285), 785–789.

(75) Frayn, K. N. *Biochem. Soc. Trans.* **2003**, *31* (Pt 6), 1115–1119.

(76) Hue, L.; Taegtmeyer, H. *Am. J. Physiol. - Endocrinol. Metab.* **2009**, *297* (3), E578–E591.

(77) Frayn, K. N.; Arner, P.; Yki-Järvinen, H. *Essays Biochem.* **2006**, *42*, 89–103.

(78) Quake, S. R.; Scherer, A. *Science* **2000**, *290* (5496), 1536–1540.

(79) Au, A. K.; Lai, H.; Utela, B. R.; Folch, A. *Micromachines* **2011**, *2* (2), 179–220.